

TALAT Lecture 1204

Precipitation Hardening

47 pages, 60 Figures

prepared by M H Jacobs *
Interdisciplinary Research Centre in Materials
The University of Birmingham, UK

Objectives

To provide an introduction to the metallurgy of precipitation hardening, with a presentation of the fundamental mechanisms involved and illustrations from alloys which form the basis for engineering alloys. The Al-Mg₂Si system is discussed in some detail because of its commercial importance. The microstructural aspects of precipitation hardening are illustrated by examples, many of which were obtained by electron microscopy; an outline of the background to electron microscopy is given in an appendix. Familiarity with the subject matter covered in earlier lectures 1201, 1202 and 1203 is assumed.

Date of Issue: 1999

© EAA - European Aluminium Association

1204 Precipitation Hardening

Contents (60 Figures)

1204 Precipitation Hardening	2
1204.01 Introduction	3
1204.02 Brief Historical Background	3
1204.03 Age Hardening - Metallurgical Background	5
1204.03.01 Precipitation from supersaturated solid solution	5
1204.03.02 Precipitation of solute clusters - Guinier-Preston zones (GP zones)	6
1204.03.03 Coherency of GP zones	9
1204.03.04 Homogeneous nucleation	10
1204.03.04.01 Homogeneous nucleation of solute clusters	10
1204.03.04.02 Stability of solute clusters	13
1204.03.04.03 Coarsening of solute clusters (Ostwald ripening)	15
1204.03.05 Slip and hardening	16
1204.03.06 Age hardening curves and the ageing sequence	17
1204.03.07 Precipitate-free zones at grain boundaries	21
1204.03.07.01 Solute depletion	21
1204.03.07.02 Vacancy depletion	22
1204.03.07.03 Asymmetrical precipitate-free zones	23
1203.03.08 Heterogeneous nucleation	24
1204.04. Age Hardening - details on Al-Mg-Si	26
1204.04.01 Pseudo-binary Al-Mg ₂ Si	26
1204.04.02 Natural ageing	31
1204.04.03 Two step ageing	32
1204.05 Age Hardening - summary of other important engineering alloys	39
1204.06 Appendix Introduction to analytical electron microscopy	40
1204.06.01 Background	40
1204.06.02 Scanning Electron Microscopy (SEM)	42
1204.06.03 Transmission Electron Microscopy (TEM)	43
1204.07 References	45
1204.08 List of Figures	46

1204.01 Introduction


This section deals with the technologically important, precipitation hardening aluminium alloys. This class of alloy contains deliberate additions of certain solute elements, for example certain combinations from Cu, Mg, Si, Mn and Zn are common solute elements, although other elements may be involved in special alloys for special applications. Upon appropriate heat treatment, the solute atoms progressively cluster together to form very small particles which separate out within the matrix grains of the alloy; this process is called precipitation. It should be clearly understood from the outset that precipitation is a metallurgical process (a phase transformation) that responds to the fact that the alloy is initially in a state far from equilibrium and, given sufficient time at temperature, diffusion of atoms occurs progressively to transform the metallurgical structure (the microstructure) towards the equilibrium situation as defined by the relevant phase diagram, the principles of which were explained in the previous [lecture 1203](#). After fast cooling and under specific conditions of heat treatment which are dealt with in detail below, the precipitation that ensues creates precipitate particles that usually provide an appreciable impediment to plastic deformation by slip; hence, as precipitation proceeds and the size and number of precipitates increases, the alloy hardens and strengthens with age (in this situation, hardness is a measure of the resistance to plastic deformation and is related to yield or tensile strength, see [lecture 1205](#)). Hence, a frequently used alternative name to **precipitation hardening** for the process is **age hardening**.

After a brief historical introduction, this chapter explains the basic principles of physical metallurgy that relate to the mechanism and process of precipitation hardening. It then goes on to provide outlines of how these metallurgical principles affect the structure and properties of aluminium alloys of engineering importance.

1204.02 Brief Historical Background

The history of precipitation hardening of aluminium alloys goes back to 1906 when A. Wilm [1] discovered that a rapidly cooled (quenched from a high temperature $\sim 550^{\circ}\text{C}$ into cold water) Al - Cu - Mg alloy initially increased in hardness as it was left at room temperature; the alloy hardened with age, which led to the phenomenon being called **age hardening**, [Figure 1204.02.01](#). Wilm examined his samples in an optical microscope, but was unable to detect any structural change as the hardness increased. It was not until 1919 and the work of Mercia, Waltenberg and Scott [2] that the beginning of an explanation was proposed. In their study of an Al - Cu alloy, they also observed a hardness increase after quenching. They demonstrated that the solid solubility of copper in aluminium decreases with decrease in temperature (as illustrated in the phase diagram shown in [Figure 1203.01.08](#)) and this led them to propose that the hardening with age after quenching was due to copper atoms precipitating out as particles from *supersaturated solid solution* (in other words, the alloy matrix after quenching contains more than the equilibrium concentration of solute atoms). In a review paper published in 1932, Mercia [3] suggested that age hardening in Al - Cu alloys resulted from the assembly of copper atoms into a random array of small clusters (“knots”) which interfere with slip when grains are deformed; for example, when the hardening associated with ageing is measured by indentation

(deformation) with a diamond indenter. The first direct evidence of Mercia's "knots" was provided in 1938 by the historic work of Guinier [4] and Preston [5] who, independently, interpreted features in diffuse x-ray scattering from aged aluminium alloys as evidence for clustering of atoms into very small zones; since termed Guinier - Preston zones, or GP zones for short.

<h2 style="text-align: center; color: red;">PRECIPITATION HARDENING</h2> <h3 style="text-align: center;">Brief history of precipitation (age) hardening</h3>		
<p>1906 A Wilm discovered that a rapidly cooled Al-Cu-Mg alloy increased in hardness as it was left at room temperature; the alloy hardened with age hence age hardening.</p> <p>1919 Mercia et al observed age hardening in Al-Cu alloy; their experiments demonstrated decreasing solid solubility of copper in aluminium with decrease in temperature during cooling they proposed that atoms assembled in clusters or "knots".</p> <p>1938 Guinier and Preston, in pioneering independent research using x-ray scattering, found evidence for clustering of atoms into what we now call Guinier-Preston zones (abbreviated to GP zones).</p> <p>1950's First direct microscopic observation of GP zones in the transmission electron microscope (eg platelet GP zones in Al-Cu by Nicholson and Nutting); small precipitate particles were observed hence precipitation hardening.</p>		
 <p>TALAT Training in Aluminium Application Technologies</p>	<p>Precipitation hardening : Historical background</p>	
<p style="text-align: right;">1204.02.01</p>		

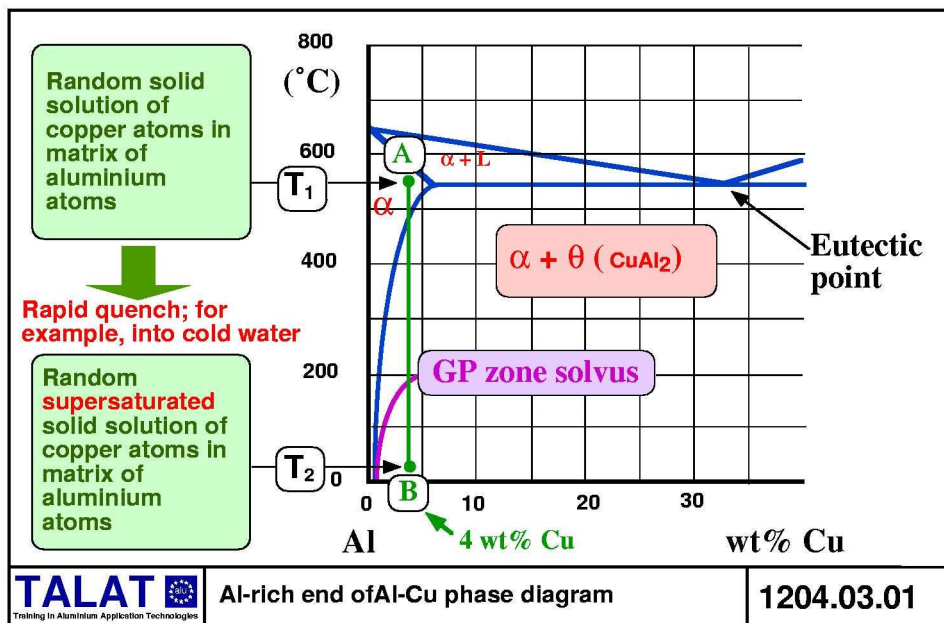
Direct observation of the precipitated GP zones did not occur until the analytical tool of transmission electron microscopy was developed in the post World War 2 era. For the first time, the transmission electron microscope provided a research technique with adequate resolution to reveal the very small precipitate particles (the GP zones) responsible for age hardening. Henceforth the terms **age hardening** and **precipitation hardening** became synonymous.

The rate and degree of hardening were found to increase if an alloy is aged at an elevated temperature, say up to 200°C; this was termed *artificial ageing* as distinct from ageing at room temperature, but current understanding of the mechanisms involved (see below) indicate that is somewhat of an unnecessary distinction and the influence of temperature is more one of effect on process kinetics rather than a fundamental change of process type. None the less, as we will see below, for some alloys (for example, Al-Mg₂Si) there may be important differences in detail between the metallurgical processes that occur at different temperatures, particularly in the sequence of phase transformations that constitute the precipitation sequence; that is, the manner in which solute clusters (zones) grow and evolve in shape and crystal structure. Details of these transformations, especially related to the very early stage of solute clustering (precipitation of GP zones) which require experimental investigation at around the atomic level, are still emerging, so it must be emphasised that there is on-going research in this area.

1204.03 Age Hardening - Metallurgical Background

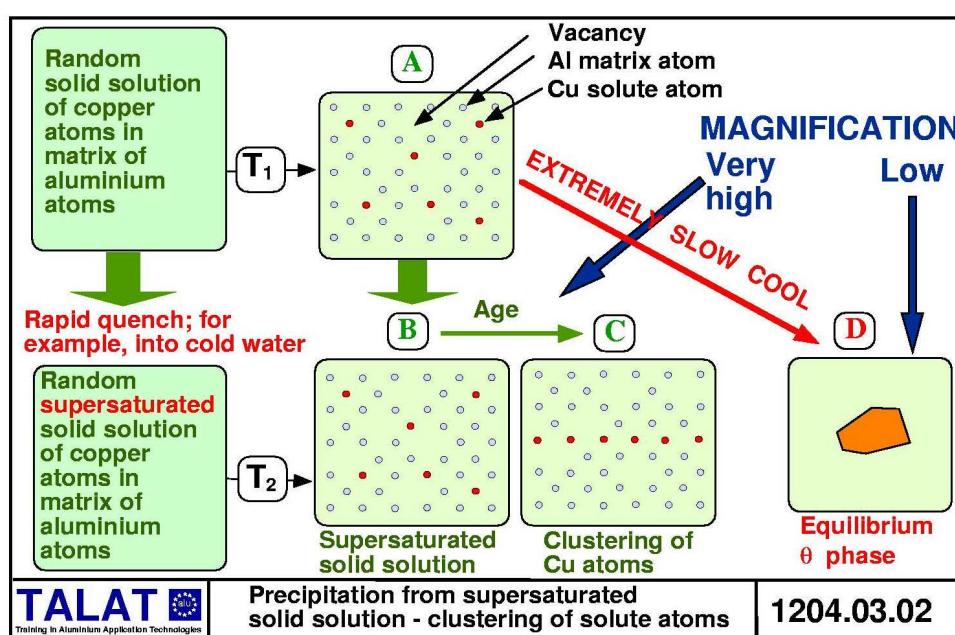
1204.03.01 Precipitation from supersaturated solid solution

The key metallurgical feature of aluminium alloys that may be hardened (strengthened) by heat treatment is complete solute solid solubility at high temperature but only very limited solute solid solubility at room temperature. Historically this was first recognised with Al - Cu alloy, so that is a good place to start. The characteristic phase diagram for Al - Cu is illustrated in [Figure 1204.03.01](#). It is a classical eutectic system; however our interest is in the aluminium-rich end of the diagram. Consider an alloy of composition Al + 4wt% Cu. At a temperature of 550°C (point A on the diagram) the equilibrium microstructure is a complete, random solid solution of copper atoms in the aluminium matrix; this is designated as α phase. This α phase will also contain a high vacancy concentration (see [lecture 1201](#)) and this allows the copper solute atoms to be mobile. In marked contrast, at room temperature and after extremely slow cooling the equilibrium microstructure consists of an extremely dilute concentration of copper in the α phase together with coarse particles of an equilibrium second phase CuAl_2 , see [Figure 1204.03.02](#) which are formed predominantly at high temperatures (say between about 450°C and 300°C during cooling). The equilibrium vacancy concentration at room temperature is extremely low, and diffusion will be practically non-existent - the equilibrium structure is stable with time at this relatively low temperature. This equilibrium structure at room temperature is not very strong and of no particular interest to an engineer or designer. However, as explained below, the situation is radically changed if the alloy is rapidly quenched, for example into water, from 550°C down to room temperature.



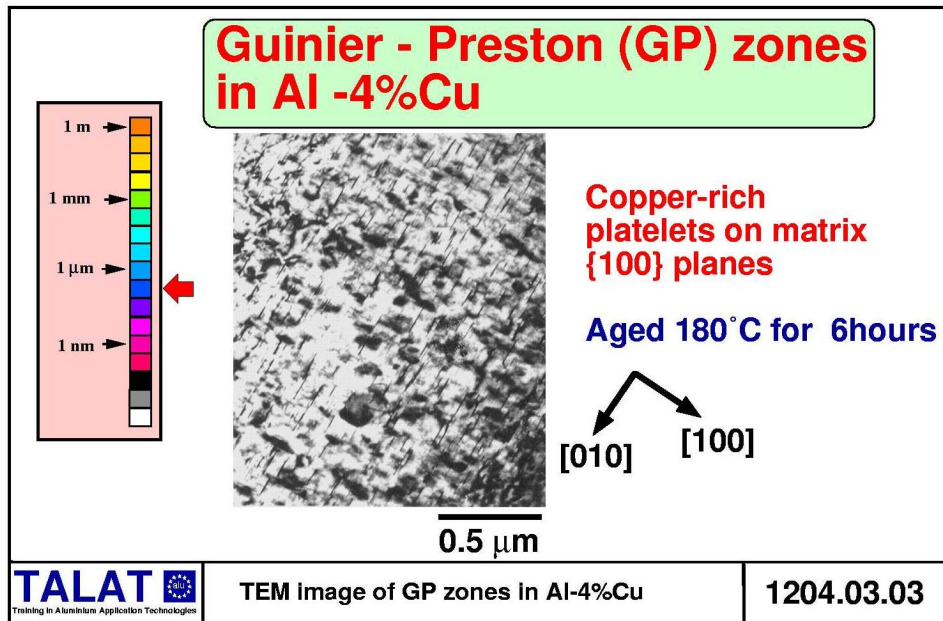
Rapid quenching from A to B (see [Figure 1204.03.01](#) and [Figure 1204.03.02](#)) freezes in the random solid solution that existed at 550°C. Of course, this cannot be an equilibrium situation; the quenched alloy is said to be in a metastable state of

supersaturated solid solution. This means that the microstructure is thermodynamically unstable, with a metallurgical driving force for the alloy to move towards the equilibrium structure - the total free energy of the system is progressively reduced as it moves towards equilibrium, but there may be a number of paths by which this may occur and we must return to this point shortly. Initially, the aluminium matrix is supersaturated in copper atoms. It is also highly supersaturated in vacancies. So what happens? A clue to the answer is provided by the observation that the alloy slowly gets harder if left for a period of time (several hours). The rate of hardening is more rapid if the alloy is heated, say to around 150°C. This is because the higher temperature allows the vacancies to be more mobile and, as a consequence, copper atoms diffuse rather more quickly. The copper atoms cluster in local groups (picture C in [Figure 1204.03.02](#)) to form the Guinier-Preston zones (GP zones) that were introduced at the start of this section. The process is called precipitation; that is, the clusters of solute atoms (the GP zones) precipitate out from solid solution.

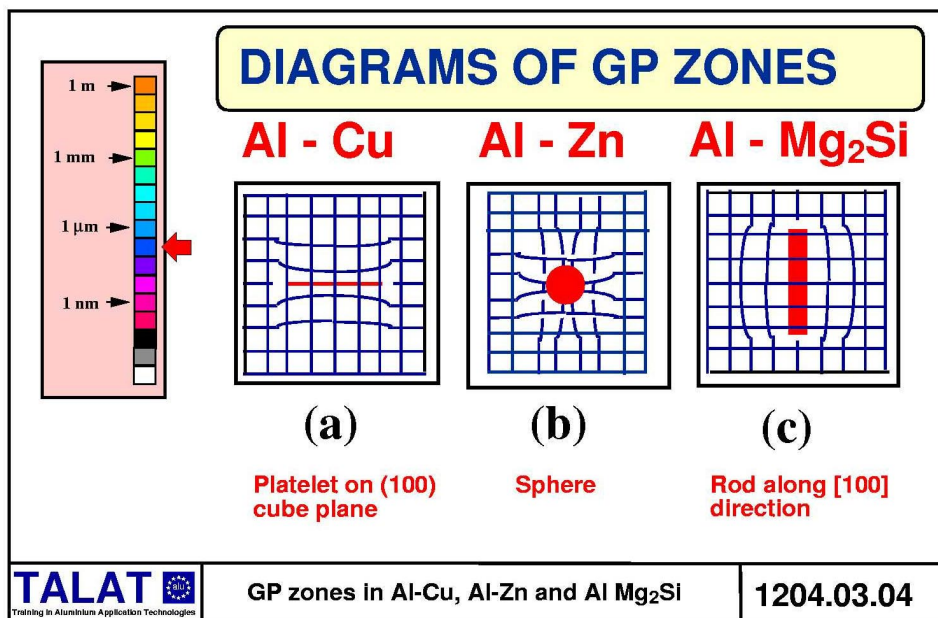


1204.03.02 Precipitation of solute clusters - Guinier-Preston zones (GP zones)

GP zones in Al-4%Cu are platelet shape; this may be seen from the transmission electron micrograph in [Figure 1204.03.03](#). The plates are very small, less than 0.1 μm in diameter, and they are precipitated on {100} planes of the aluminium matrix. To understand the reason for the platelet shape, remember that in [lecture 1201](#) and [Figure 1201.03.02](#) and [Figure 1201.03.03](#) it was pointed out that copper atoms are smaller than aluminium atoms (by about 10%). Hence, when they cluster together as a one-atom thick layer on a matrix cube plane, the matrix distorts around the platelet, see diagram (a) in [Figure 1204.03.04](#). It is this lattice distortion that provides the main contribution to the imaging process [6] in the Transmission Electron Microscope (TEM). The basic principles of electron microscopy are outlined in the appendix to this lecture.

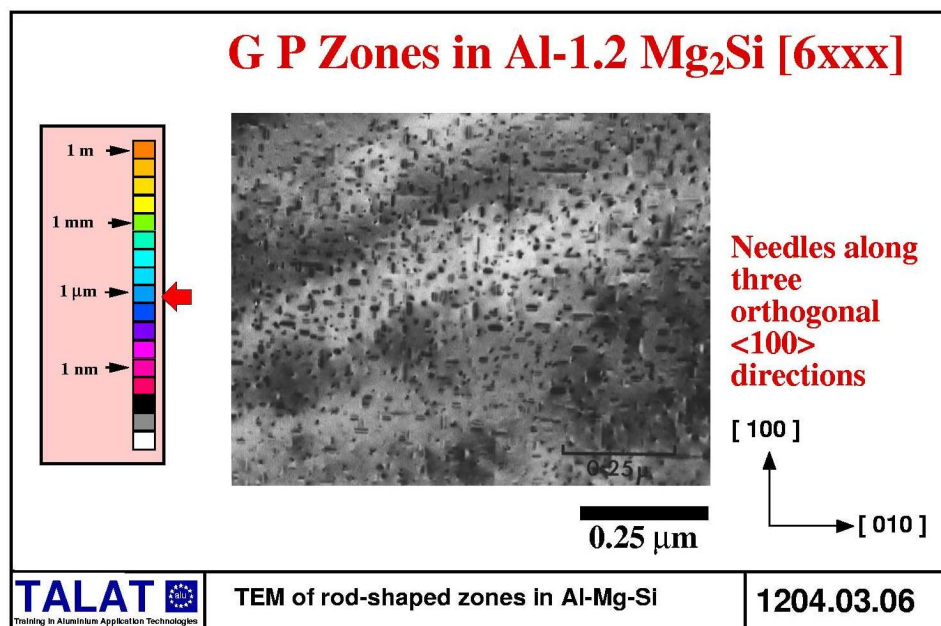
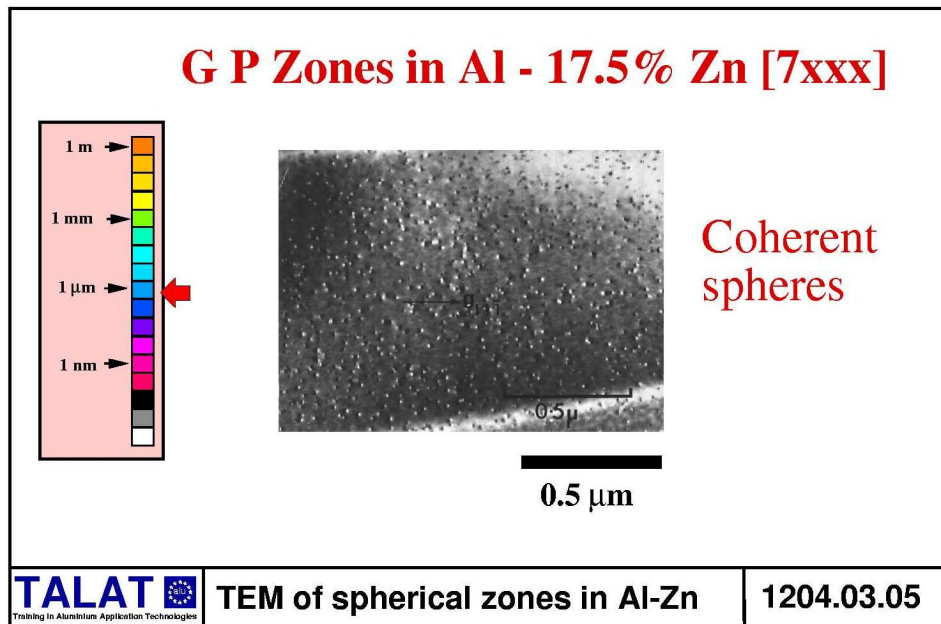


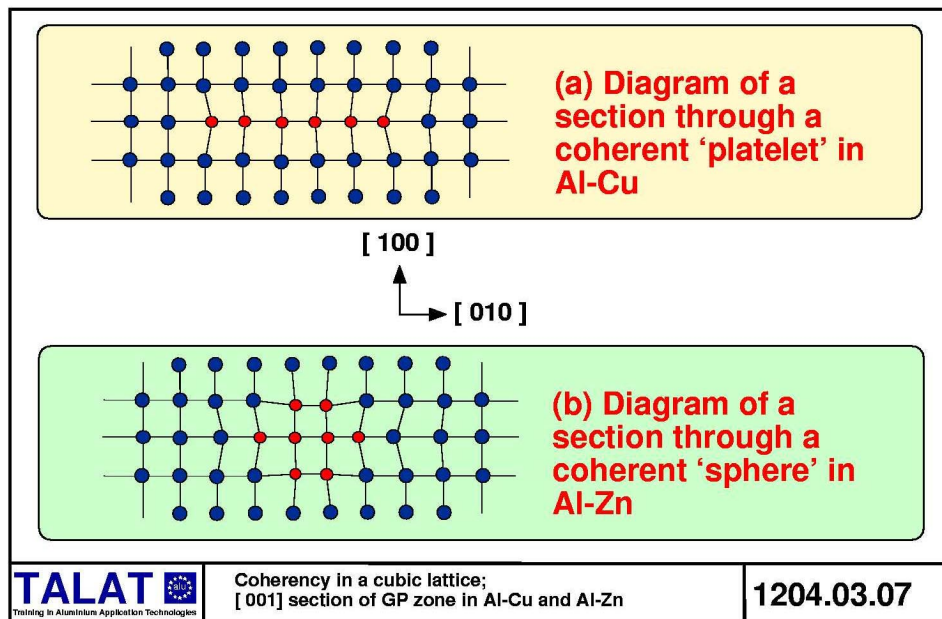
In a similar way, Al-Zn alloys can be quenched and aged to produce GP zones. In this case the size difference between Al and Zn atoms is only approximately 3.5%, and the zones are approximately spherical in shape, shown diagrammatically as (b) in [Figure 1204.03.04](#) and in the TEM micrograph, [Figure 1204.03.05](#). Again, it is the small lattice distortion that mainly allows these very small zones to be imaged in the TEM.



Al-Mg-Si is a very important engineering alloy for structural applications, and it happens to provide a third, different shape of GP zone - in this case rods along the three, cube $\langle 100 \rangle$ directions of the aluminium matrix, shown as diagram (c) in [Figure 1204.03.04](#) and in the TEM micrograph, [Figure 1204.03.06](#). Relative to an Al atom, a Mg atom is about 10% larger and a Zn atom is approximately 21% smaller, so it might be expected that the Mg and Si atoms would associate and precipitate

together - this is broadly what happens (although we will need to look in more detail at this later in this chapter).



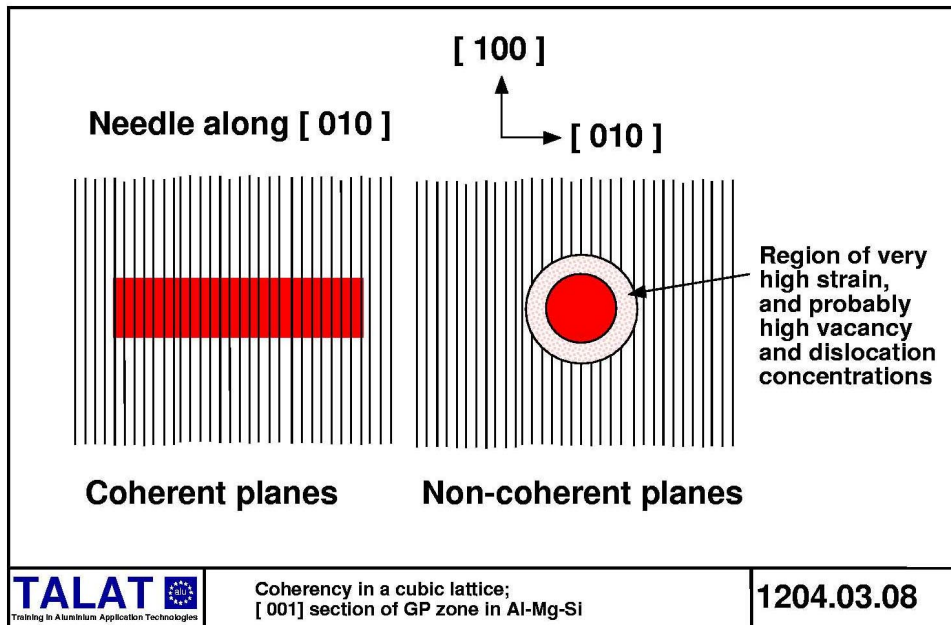


1204.03.03 Coherency of GP zones

An important concept in the understanding of how GP zones harden an aluminium alloy is the fact that the GP zones are composed of clusters of solute atoms that are said to be coherent with the aluminium lattice. For Al-Cu, this is illustrated in (a) of [Figure 1204.03.07](#) - the copper atoms assemble in single atom layers on {100} planes, which creates a distortion, in this case a contraction, of the lattice (remember, Cu atoms are smaller than Al atoms). Nonetheless, continuity of the crystallographic planes is maintained; the platelets of copper are fully coherent with the aluminium lattice.

GP zones in Al-Zn are also fully coherent, see (b) in [Figure 1204.03.07](#). Here, the zones are approximately spherical in shape and, because Zn atoms are slightly smaller than Al atoms, the distortion is again a contraction of the lattice. However, the zones are again fully coherent.

GP zones in Al-Mg-Si are only semi-coherent, [Figure 1204.03.08](#). The needle-shaped (or rod-shaped) zones are coherent with the matrix along their length, which is along a aluminium matrix $\langle 100 \rangle$ direction. Detailed electron microscopy with a Field Emission Gun Scanning Transmission Electron Microscope [7] has shown that, even when the zones are very small, they have a hexagonal structure [8] with the close-packed planes parallel to, and coherent with, the cube planes of the aluminium matrix. There is considerable mis-match in crystal structures perpendicular to the major axis of the needle-shaped zone, associated with the "cylindrical" interface between the needle and the surrounding matrix; the matrix in the neighbourhood of the cylindrical interface expands to accommodate the mismatch.

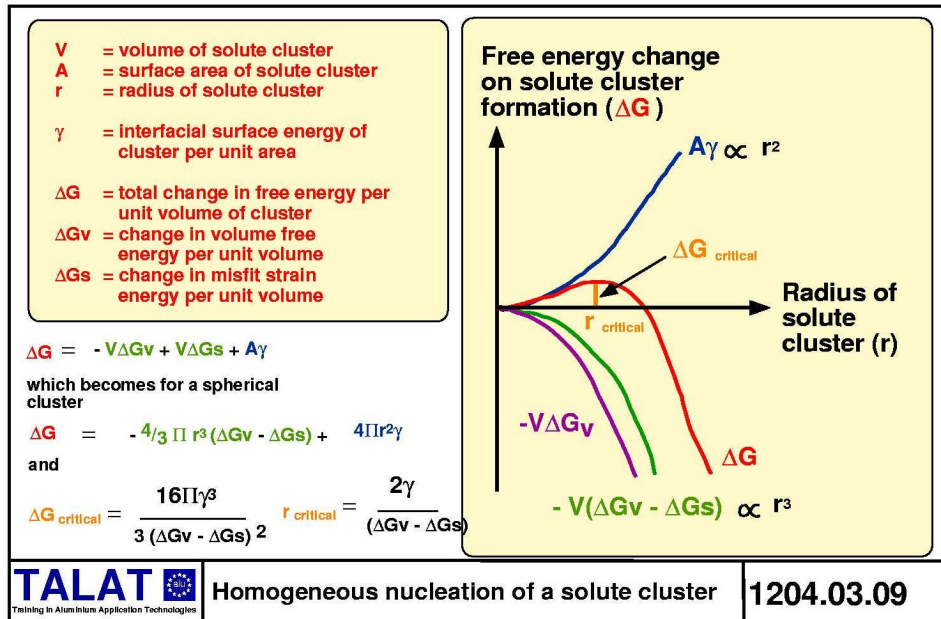


1204.03.04 Homogeneous nucleation

The solute clusters discussed and illustrated above form randomly within the crystalline matrix of the supersaturated solid solution. This process is called homogeneous nucleation. We have seen above that, in the cases of Al-Cu and Al-Zn, the clusters form in a strained fcc array coherently within the fcc lattice of the supersaturated matrix. In the case of Al-Mg₂Si, the needle-shaped zones are coherent only along their major axes, with highly-strained, non-coherent interface regions perpendicular to the major axes of the needles. Consequently, the needles are said to be “semi-coherent”. However, in all three cases, the interfaces between the clusters of solute atoms and the surrounding matrices are of lower energies than those which correspond to the interfaces between the corresponding equilibrium phases and the matrices. Note that a high interfacial energy is characterised by a highly-strained interface, with a high local atomic disorder. Creation of such an interface presents a considerable barrier to the homogeneous nucleation of an equilibrium phase within the supersaturated matrix. Consequently, clusters of solute atoms are formed which provide some relief of the supersaturation and which, because they have lower interfacial energies with the matrix, are easier to nucleate. This concept is fundamental to the understanding of homogeneous nucleation of solute clusters. An outline of the basic theory of homogeneous nucleation is presented below.

1204.03.04.01 Homogeneous nucleation of solute clusters

It is a basic law of nature that any system will strive to move towards its lowest free energy state, when it is said to be in equilibrium with its surroundings. This is the situation that is presented on an equilibrium (or phase) diagram. The free energy change associated with the homogeneous nucleation of solute clusters has three contributions, see [Figure 1204.03.09](#):



1. The creation of a volume V of clustered solute atoms gives rise to a volume free energy **reduction** of $V\Delta G_v$ where ΔG_v is the change in volume free energy per unit volume.
2. The creation of an area A of interface between the solute cluster and the matrix produces an **increase** in free energy of $A\gamma$, where γ is the energy per unit area of the interface between the cluster and the matrix (in this simplified presentation of the theory we will assume that γ is isotropic).
3. Because of a difference in sizes between the solute atoms and those of the matrix there is a volume strain associated with a cluster, corresponding to an increase of free energy of $V\Delta G_s$, where ΔG_s is change in misfit strain energy per unit volume.

Hence, the total free energy change, ΔG , associated with the formation of a cluster of solute atoms is given by [8 and 9]:

$$\Delta G = -V\Delta G_v + A\gamma + V\Delta G_s \quad (3.4.1)$$

In order to keep the geometry simple, let us assume that the solute cluster is spherical in shape (i.e. let us consider the simple picture for solute clusters in Al-Zn). If r is the radius of the cluster, then equation 3.4.1 gives

$$\Delta G = -\frac{4}{3}\pi r^3(\Delta G_v - \Delta G_s) + 4\pi r^2\gamma \quad (3.4.2)$$

Equation 3.4.2 is shown plotted in **Figure 1204.03.09**. It will be seen that, with increasing cluster radius r , ΔG initially **increases** to a maximum $\Delta G_{critical}$ at a critical radius $r_{critical}$, after which ΔG **decreases**. Because, overall, the system needs to decrease its free energy, the initial increase represents an energy barrier that has to be overcome for a stable cluster to be formed - **there is a barrier to nucleation**.

Differentiation of equation (3.4.2) with respect to r and setting the result to equal zero (the mathematical criterion for a maximum) gives the value of r_{critical} as

$$r_{\text{critical}} = 2\gamma / (\Delta G_v - \Delta G_s) \quad (3.4.3)$$

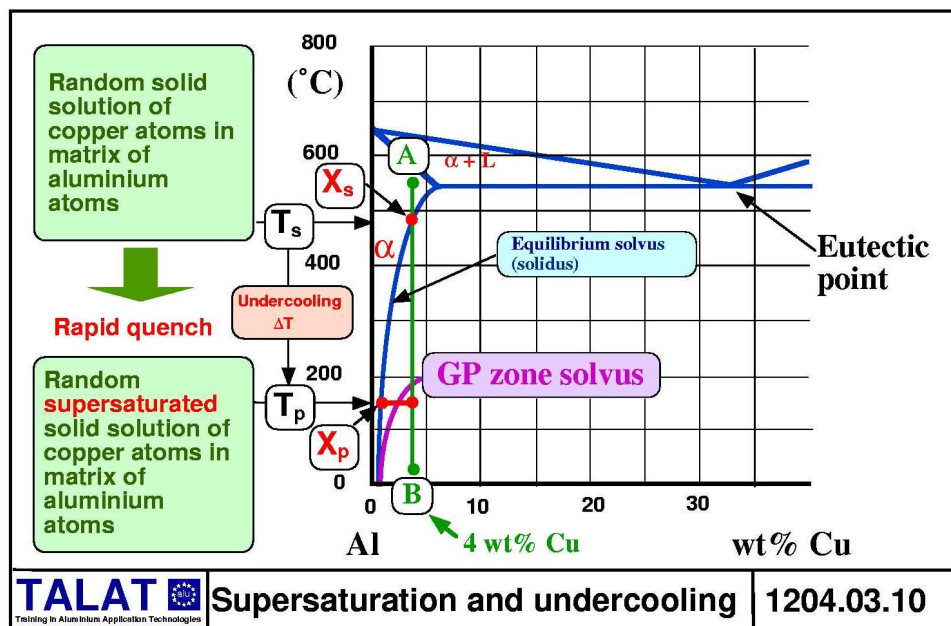
Substitution of r_{critical} in (3.4.2) gives

$$\Delta G_{\text{critical}} = 16\pi\gamma^3 / 3(\Delta G_v - \Delta G_s)^2 \quad (3.4.4)$$

So what does this tell us ? We note two important features:

1. The critical radius for nucleation, r_{critical} , decreases according to the decreasing value of the interfacial energy γ . This means that, in general terms, the critical radius is smaller for a solute cluster with a coherent (low energy) interface compared with one with an incoherent (high energy) interface.
2. The effect of the strain energy term (ΔG_s) is to reduce the effective driving force for cluster formation. It will be seen that this strain energy term has the effect of reducing the value of the expression ($\Delta G_v - \Delta G_s$) in the denominator of equation (3.4.3). Through (3.4.3), this has the effect of increasing the size of the critical radius.

Hence, the possibility that a random fluctuation of solute atoms will lead to a cluster larger than the critical size for stability will be favoured in a system where the clusters are fully coherent and of small volume strain. Furthermore, the degree of supersaturation is a measure of the driving force for precipitation - where the term 'supersaturation' is given approximately by the following relationship [9,10] which is illustrated in [Figure 1204.03.10](#).



Supersaturation at temperature T_p is given by

$$S_p = X_s / X_p \quad (3.4.5)$$

where X_s = the equilibrium concentration of solute atoms at temperature T_s ,
(which is equal to the initial concentration of solute atoms in the
matrix after heat treatment, see point A in [Figure 1204.03.10](#))
and X_p = the equilibrium concentration of solute atoms at temperature T_p
(where T_p corresponds to the temperature after quenching)

Also, we note that the driving force for precipitation is given by

$$\Delta G_v \propto (X_s - X_p) \quad (3.4.6)$$

We see therefore that the driving force for cluster formation (precipitation) increases with increasing undercooling (ΔT) created by the rapid quench (i.e. a decrease of X_s).

In practical terms, the temperature T_p must be low enough such that the magnitude of the supersaturation is such that there is a high probability of stable clusters being formed - that is, in the context of this lecture, GP zones are formed. Accordingly, a curve is often drawn on the phase diagram to represent the upper bound of GP zone formation - the so-called **GP zone solvus**, see [Figure 1204.03.10](#). It must clearly be understood that inclusion of a GP zone solvus line on a phase diagram is for convenience of understanding and for guiding heat treatment procedures. The GP zone solvus is not an equilibrium curve and must be seen as an annotation to the phase diagram and strictly not part of it - it is however, very useful, particularly when coupled with its associated stability curves which are discussed below in section 3.4.2.

Finally, it must be emphasised that the description above for spherical solute clusters (zones) is for the sake of geometrical simplicity and ease of mathematical presentation. In general terms, the basic concepts apply to all other zone shapes.

1204.03.04.02 Stability of solute clusters

Two further points must be made concerning the factors that determine the stability of a solute cluster.

Firstly, the brief outline of the factors that determine homogeneous nucleation of a solute cluster given above assumes that the event is isolated and that the surrounding supersaturation may be regarded as constant. In practice, during real age hardening, there is usually a high population density of clusters. Hence the clustering processes are coupled and the supersaturation surrounding the clusters decreases very significantly. This is because the process of clustering itself drains solute atoms from the matrix. Thus the effective supersaturation (S) will be less than the supersaturation (S_p) prior to the onset of clustering.

Secondly, because the clusters are so small, there may be a significant influence of the curvature of a given cluster of radius r on its stability at a given temperature T in a given effective supersaturation (S) as defined in the paragraph above. It can be shown

[9,10] that this relationship is given by the Gibbs-Thompson equation (this is sometimes called the Gibbs-Freundlich equation), **Figure 1204.03.11**, as follows

$$\ln S = \ln X_r / X_p = 2\gamma\Omega / r kT \quad (3.4.7)$$

where X_r is the concentration of solute in equilibrium with a solute cluster of radius r , X_p is the equilibrium solute concentration as defined by the solidus of the phase diagram,

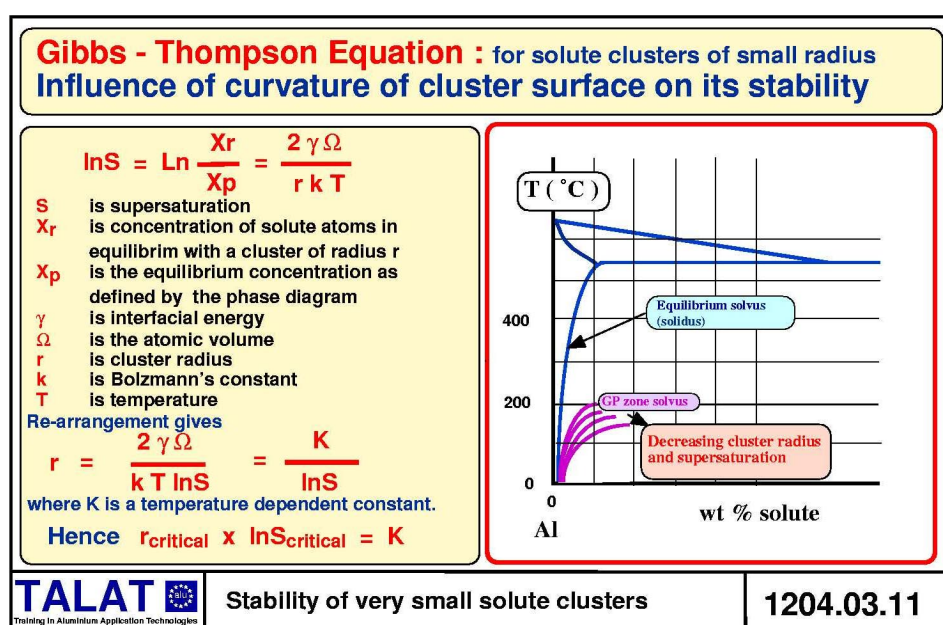
Ω is the atomic volume and k is Boltzmann's constant.

This equation shows that the real solute concentration in equilibrium depends on the mean radius of the clusters. At high radii, the real equilibrium concentration approaches the theoretical concentration given by the solidus curve while at small radii, the real equilibrium concentration can reach a value much larger than the theoretical equilibrium concentration. In other words, only big precipitates are stable at small supersaturations.

For a given supersaturation, re-arrangement of equation (3.4.7) allows us to calculate the critical radius ($X_r = X_s$)

$$r_{\text{critical}} = 2\gamma\Omega / kT \ln X_r / X_p = K / \ln X_s / X_p = K / \ln S \quad (3.4.8)$$

where K is a temperature dependent constant



Hence, the critical radius for cluster stability is inversely related to the natural logarithm of the supersaturation. This is very important, because it means that the critical radius for stability is not a constant but it is a variable, depending upon the ageing temperature and the effective supersaturation, which itself is dependent upon the number and size distribution of clusters. Consequently, there is not a unique stability curve for zones, but a family of curves, see **Figure 1204.03.11**, which represent combinations of zone size distributions and different levels of

supersaturation. In this respect, it should be noted that further rearrangement equation (3.4.8) gives

$$r_{\text{critical}} \times \ln S_{\text{critical}} = K \quad (3.4.9)$$

This emphasises the dependence of the critical radius of a zone on the local magnitude of the supersaturation.

We will return to equation 3.4.9 later in this lecture when we consider ageing at two different temperatures - for example, two step ageing when a sample is aged for a period at some low temperature (for example, room temperature) before subsequent ageing at a higher temperature; do the zones remain stable and continue to grow or are they unstable and therefore dissolve ? The answer to this question and the mechanisms involved are discussed in section 4.3 for Al-Mg₂Si alloys.

Finally, the vital role played by vacancies in stable cluster formation and growth must not be ignored. Firstly, vacancy mobility provides the fundamental mechanism for solute diffusion and hence the migration of solute atoms into clusters; hence the (non-equilibrium) vacancy concentration directly influences the kinetics of clustering. If the local supersaturation of vacancies is reduced because of the proximity of a vacancy sink (for example, a grain boundary) then it would be expected that the local kinetics of clustering would be reduced - this is indeed the case as can give rise to so-called precipitate-free zones, which are discussed later in section 3.8. Secondly, a zone where the solute cluster locally expands the aluminium matrix (for example, around a needle in Al - Mg₂Si) might be expected to trap vacancies in order to help relieve some of the local strain.

The dependence of solute mobility (diffusion rate) on the vacancy concentration is also very important because it controls the way in which the size and number distributions of solute clusters develop with time; there is a coarsening reaction known as Ostwald ripening.

1204.03.04.03 Coarsening of solute clusters (Ostwald ripening)

As time increases at a given temperature, there is a progressive decrease in the solute concentration retained in the aluminium matrix as the equilibrium supersaturation decreases towards **unity**. We have seen above that the supersaturation in metastable equilibrium with a very small cluster is larger than that in metastable equilibrium with a larger cluster. Thus, as the overall concentration of solute in the matrix progressively decreases, it will decrease to values where the radii of small clusters become less than the critical size for stability - these clusters then dissolve. Larger clusters continue to grow, so there is an overall coarsening of the size distribution of clusters.

The kinetics of the coarsening reaction (Ostwald ripening) are controlled by the diffusion rate of solute atoms in the aluminium matrix. The situation is shown schematically in **Figure 1204.03.12**.

Ostwald ripening : coarsening of solute clusters	
<p>From Figure 1200A.04.12</p> $r = \frac{2 \gamma \Omega}{k T \ln X_r / X_p} = \frac{K}{\ln X_r / X_p} \quad (1)$ <p>Also, it may be shown [10] that the variation of growth rate with radius is dependent upon the diffusion rate D of solute atoms</p> $\frac{dr}{dt} = - \frac{D (X_r - X_m)}{r} \quad (2)$ <p>X_m is the average solute concentration in the matrix</p> $\frac{dr}{dt} = \frac{K D X_p}{r} \left\{ \frac{1}{r_m} - \frac{1}{r} \right\} \quad (3)$ <p>r_m is the mean radius of solute clusters</p>	<p>Equation (3) gives variation in cluster growth / dissolution rate as a function of cluster radius r</p>
	Coarsening of solute clusters : Ostwald ripening 1204.03.12

The rate of change of cluster radius r with time is given by

$$dr / dt = - D (X_r - X_m) / r \quad (3.4.10)$$

where X_m is the mean solute concentration in the matrix.

In reference [10] it is shown how equations 3.4.8 and 3.4.10 may be developed to derive the expression

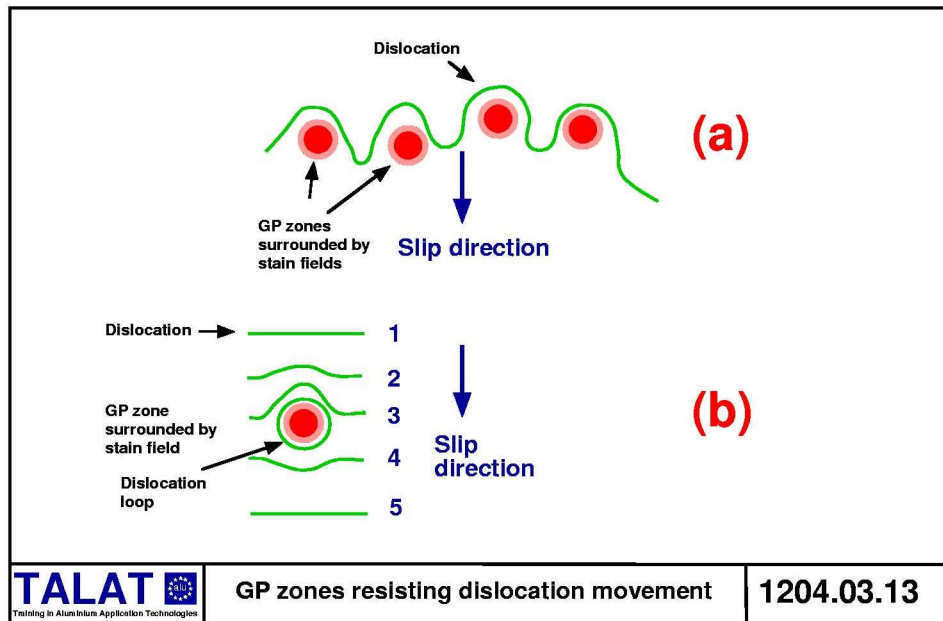
$$dr / dt = [KDX_p / r] \{ 1/r_m - 1/r \} \quad (3.4.11)$$

where r_m is the mean radius of solute clusters. Equation 3.4.11 gives the variation in cluster growth as a function of cluster radius - the relationship is shown schematically in **Figure 1204.03.12**, where it will be seen that very small clusters are unstable and dissolve while the remaining, larger clusters continue to grow. Solute atoms released into the matrix by the dissolving clusters diffuse to the larger clusters to feed their further growth. As a consequence, there is a coarsening of the distribution; the mean size of the clusters increases while the overall number of clusters decreases.

1204.03.05 Slip and hardening

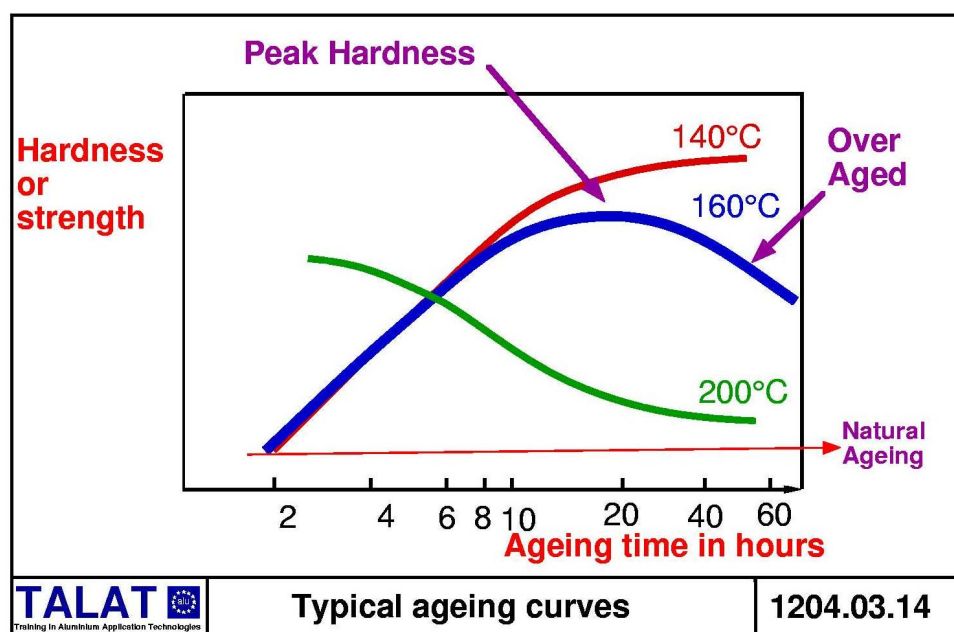
GP zones, with their associated surrounding strain fields, present impediments to slip by dislocation movement, **Figure 1204.03.13**. When the zones are small and few in number, the fact that they have a coherency relationship means that, with adequate applied stress, the dislocations may pass through zones, leaving a loop of dislocations (so-called Orowan loops) in their wake, **Figure 1204.03.13**. As ageing time increases, the zones will increase in size and slip becomes progressively more difficult - the alloy age hardens. For even longer ageing times, coarsening of clusters occurs

and slip becomes easier - the alloy softens. These features are revealed by progressive measurements of hardness to yield an age hardening curve.



1204.03.06 Age hardening curves and the ageing sequence

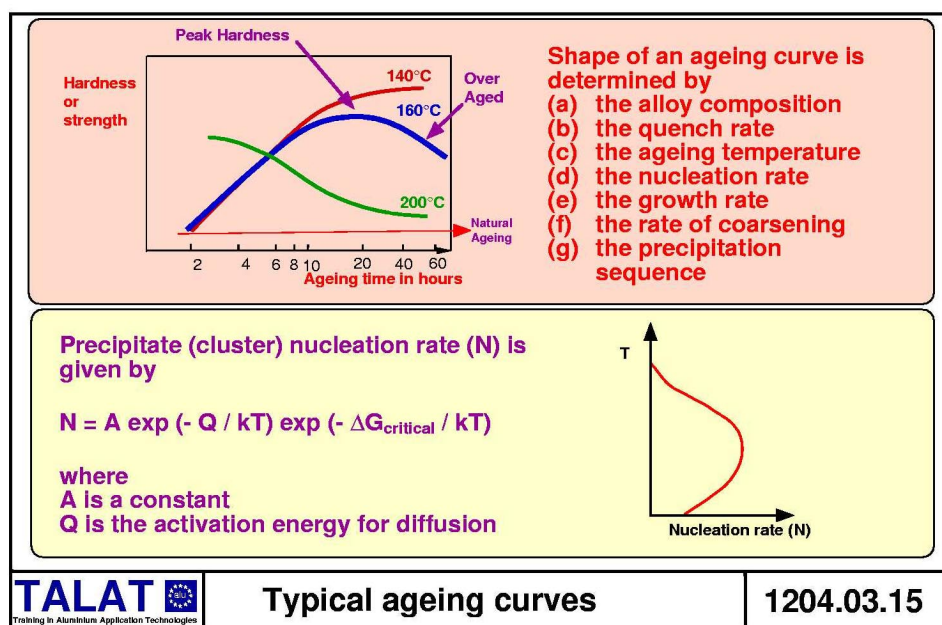
Typical age hardening curves are shown in [Figure 1204.03.14](#). Hardening at room temperature, natural ageing, although by no means insignificant, is very slow with time. More rapid, and more appreciable hardening occurs at elevated temperatures, see curve for 140°C. With ageing at 160°C, the curve illustrated schematically in [Figure 1204.03.14](#) achieves a peak hardness after about 24 hours, and thereafter softens.



At a higher temperature, for example at 200°C in [Figure 1204.03.14](#), a lower peak hardness is reached quickly and thereafter rapid softening occurs.

What basic effects control the level of peak hardness and why does an alloy soften after attaining peak hardness ? The answers lie in the combination of effects, [Figure 1204.03.15](#) (b) of

- (a) the alloy composition
- (b) the quench rate
- (c) the ageing temperature
- (d) the kinetics of homogeneous cluster nucleation
- (e) the growth rate of clusters
- (f) the coarsening reaction as ageing proceeds
- (g) the precipitation sequence - the transformations that the precipitates progress through as ageing proceeds.



The first point to note is that GP zones will only be formed if the alloy is quenched below a certain temperature, often defined by reference to the GP zone solvus and its associated family of stability curves, [Figure 1204.03.11](#). In general terms, the faster the quench and the lower the temperature between, say, 200°C and room temperature, the higher will be the nucleation rate of clusters. At lower temperatures, a decrease in solute atom mobility causes the nucleation rate to decrease (see [Figure 1204.03.15](#) (b)).

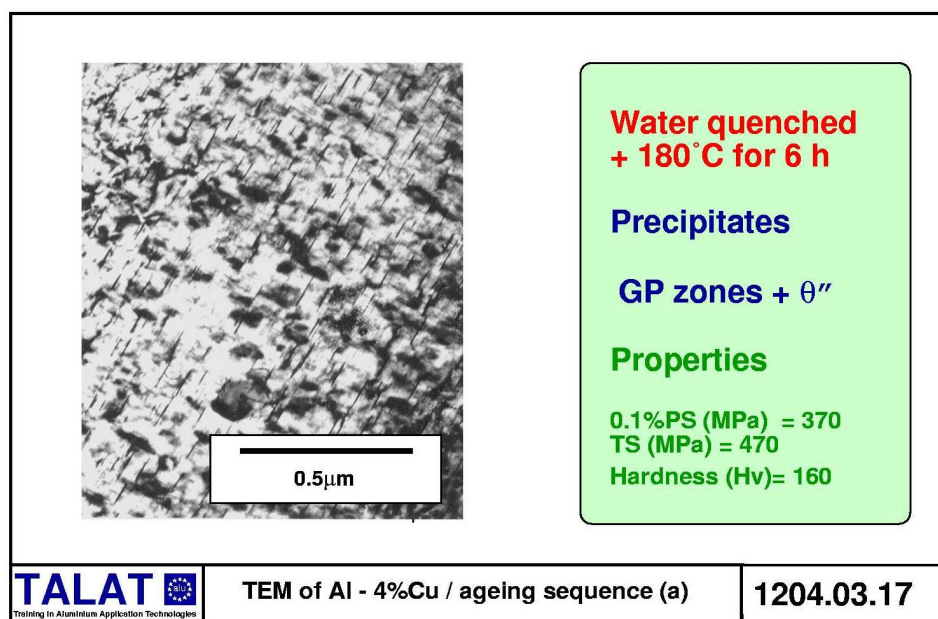
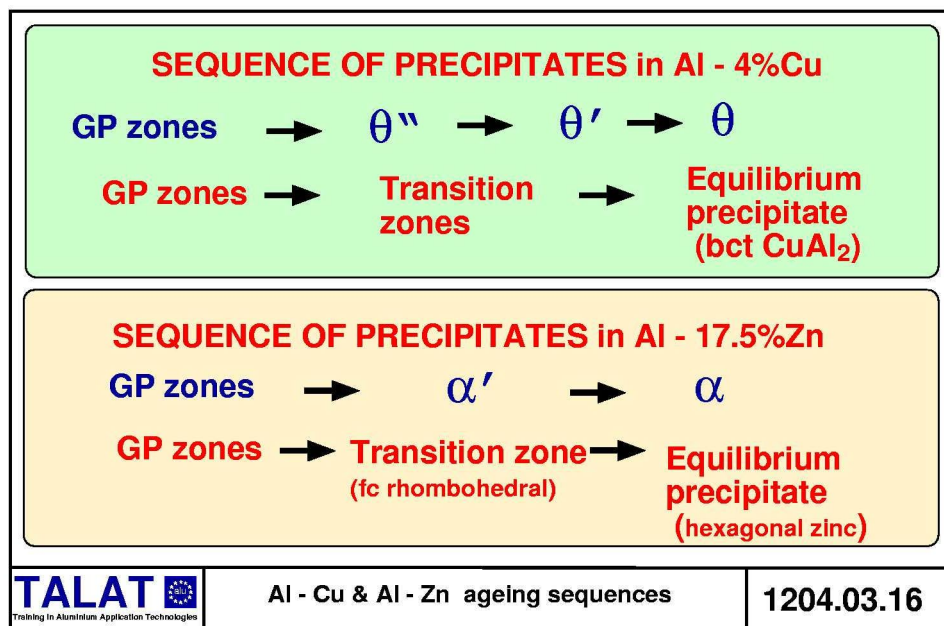
The second important point is that, as GP zones increase in size they transform to another, usually a sequence of other, intermediate phases in a progression towards the final equilibrium phase of the particular alloy system. For the case of Al-4% Cu, this is illustrated in [Figure 1204.03.16](#). The precipitation sequence is [11]:

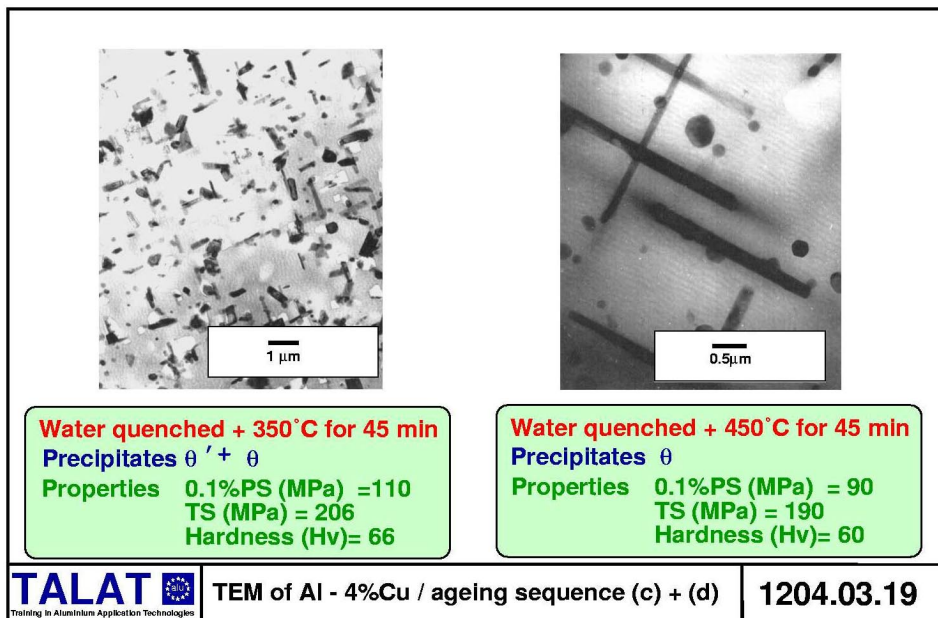
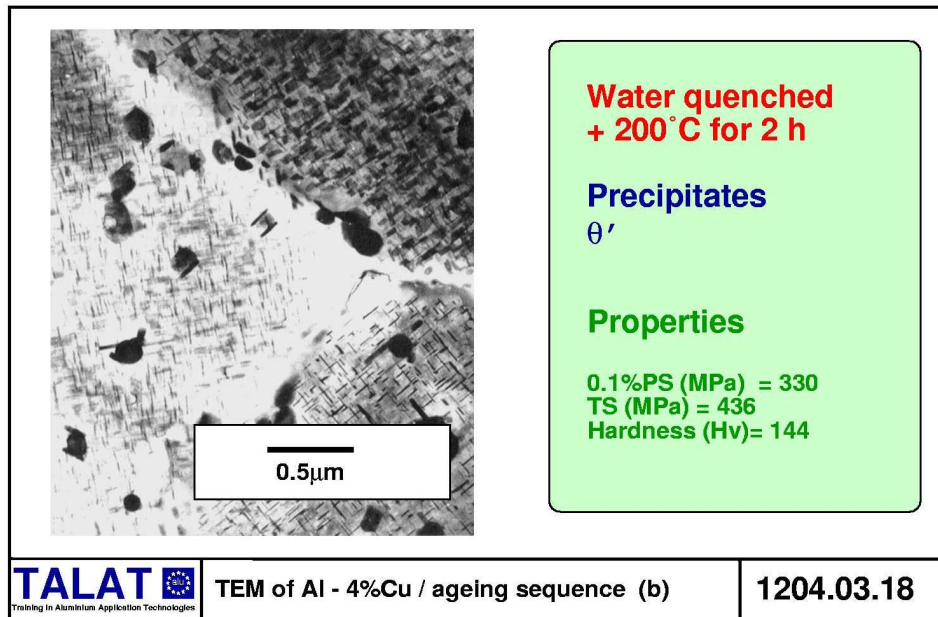


where

- θ'' are platelets of a few atomic layers thickness
- θ' are platelets of several atomic layers, some incorporating Al atoms and with a tetragonal crystal structure
- θ are thick plates of the equilibrium CuAl_2 body-centred tetragonal phase.

This sequence is illustrated in [Figure 1204.03.16](#), [Figure 1204.03.17](#), [Figure 1204.03.18](#), and [Figure 1204.03.19](#).





The sequence is best explained [11] by the premise that the precipitation follows initially the path of minimum activation energy rather than maximum loss of free energy. In other words, the kinetics favour homogeneous nucleation with a coherent interface, followed by transformation to one or more intermediate semi-coherent phases before final transformation to the equilibrium precipitate.

Al-Zn follows a similar pattern of behaviour, see [Figure 1204.03.16](#):

spherical GP zones $\rightarrow \alpha' \rightarrow \alpha$

where

α' is a intermediate face-centred rhombohedral phase

and

α is the equilibrium phase (hexagonal zinc with a very small concentration aluminium in solid solution).

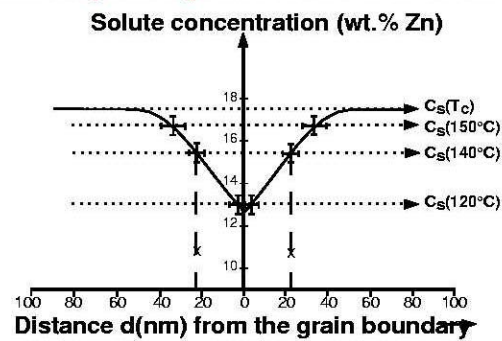
1204.03.07 Precipitate-free zones at grain boundaries

Precipitate-free zones (PFZs) adjacent to grain boundaries may be formed by several mechanisms; for example, local depletion of solute concentration, local depletion of excess vacancy concentration, and migration of the grain boundary during ageing. These are considered in turn below.

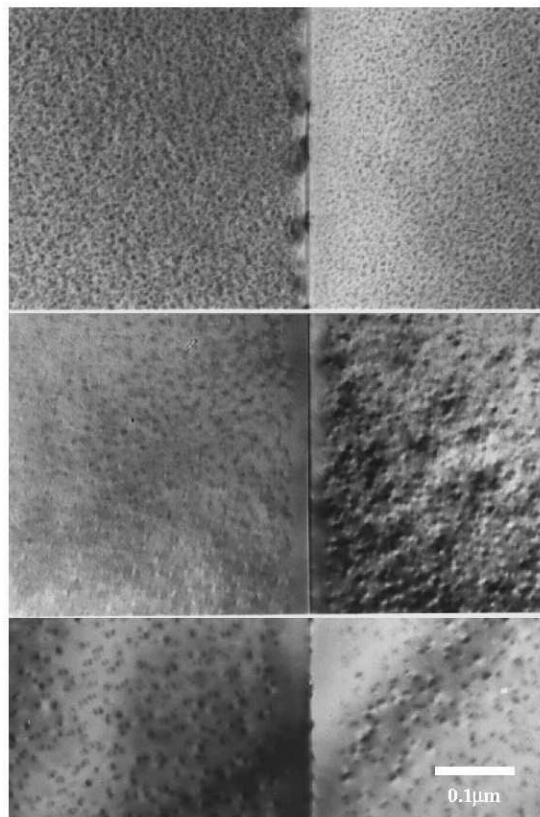
1204.03.07.01 Solute depletion

Equilibrium precipitates (maybe intermediate precipitates also) will grow at grain boundaries if an alloy is held just below the solution treatment temperature, but well above the GP zone solvus. This depletes the regions in the vicinity of the grain boundary of solute atoms - a concentration gradient is set up. The situation is shown schematically in [Figure 1204.03.20](#), for an Al-17.5%Zn alloy [12]. Note that the width of the PFZ increases with increase in the temperature of ageing, which is to be expected since the level of solute supersaturation decreases with increase in temperature.

Grain boundary Precipitate-free Zone - solute depletion



**Direct
quench
into oil**



**Aged at
120°C for
2 hours**

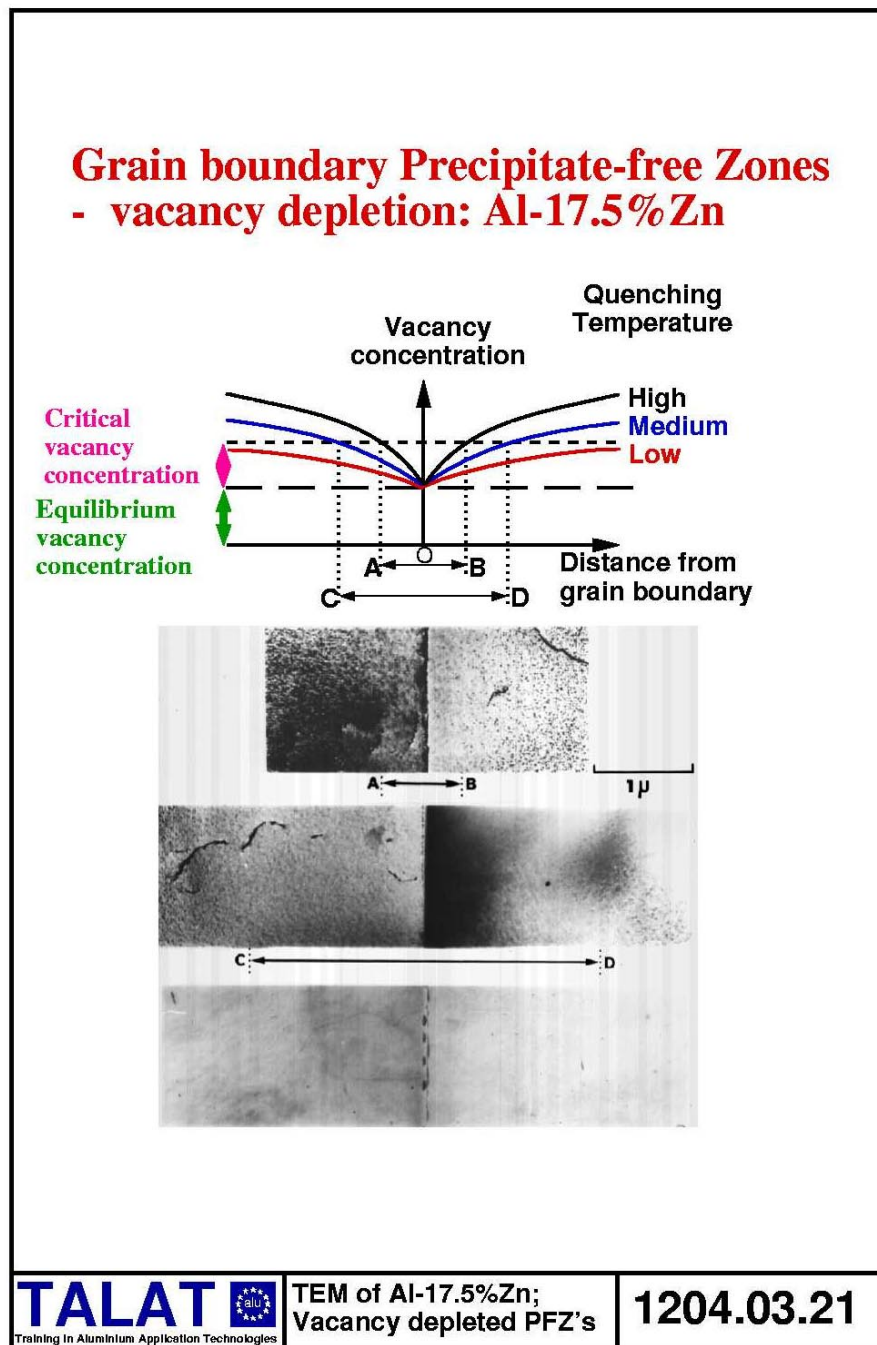
**Aged at
140°C for
2 hours**

**Aged at
150°C for
1.5 hours**

1204.03.07.02 Vacancy depletion

After quenching, we have already seen that the aluminium matrix is supersaturated in vacancies. Grain boundaries act as very efficient sinks for excess vacancies. Consequently, a concentration gradient in vacancies is established on both sides of a grain boundary. Because the local vacancy concentration directly controls the rate of solute diffusion, and this affects the rate of nucleation, it has a dramatic effect on the local rate of clustering and GP zone formation. This is illustrated in **Figure**

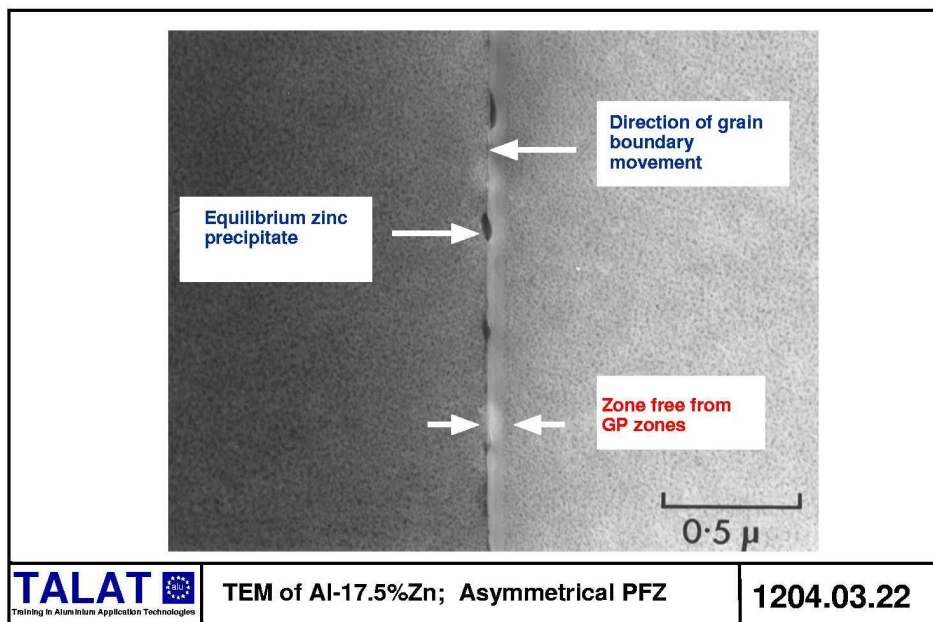
1204.03.21 for high medium and low quenching rates (see [12] for details) which, respectively, give rise to progressively wider PFZs.



1204.03.07.03 Asymmetrical precipitate-free zones

In general, precipitation inhibits grain movement. However, if grain migration does occur - for example, during cooling of a material with an abnormal grain structure, then solute may be 'swept up' by the moving boundary, which will give rise to asymmetrical solute profiles. This asymmetry is reflected in the age hardened material

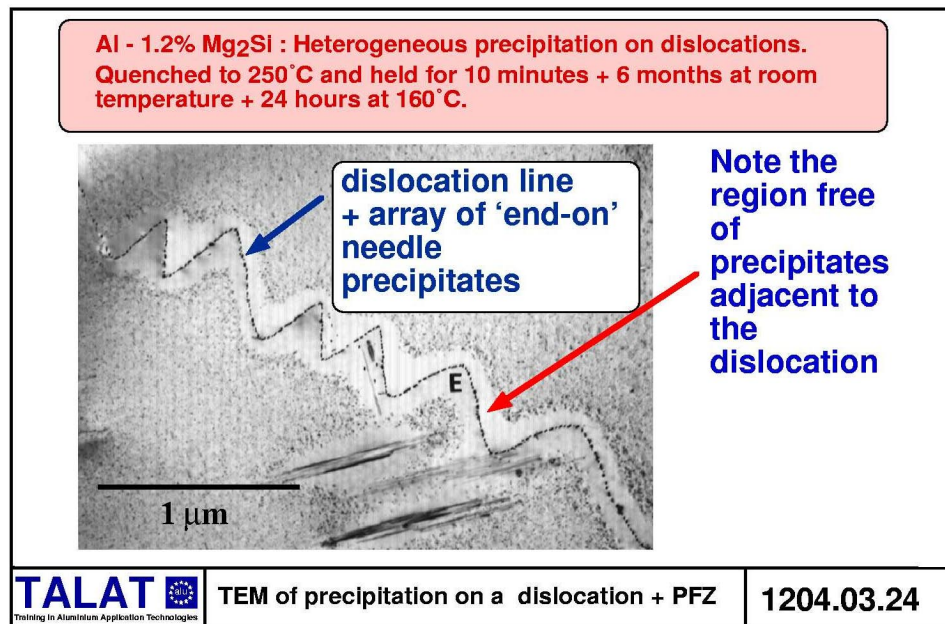
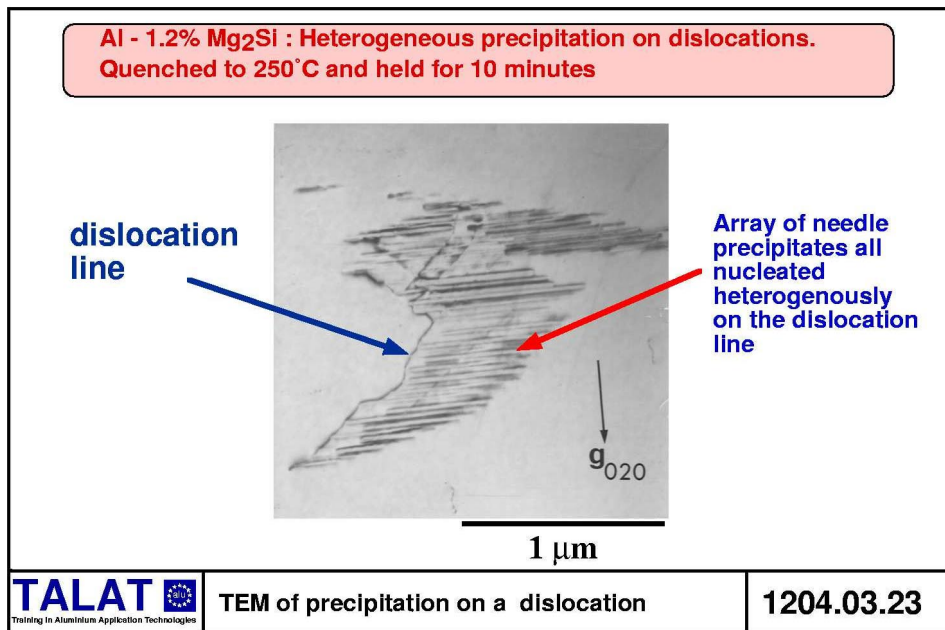
- see **Figure 1204.03.22**.



1203.03.08 Heterogeneous nucleation

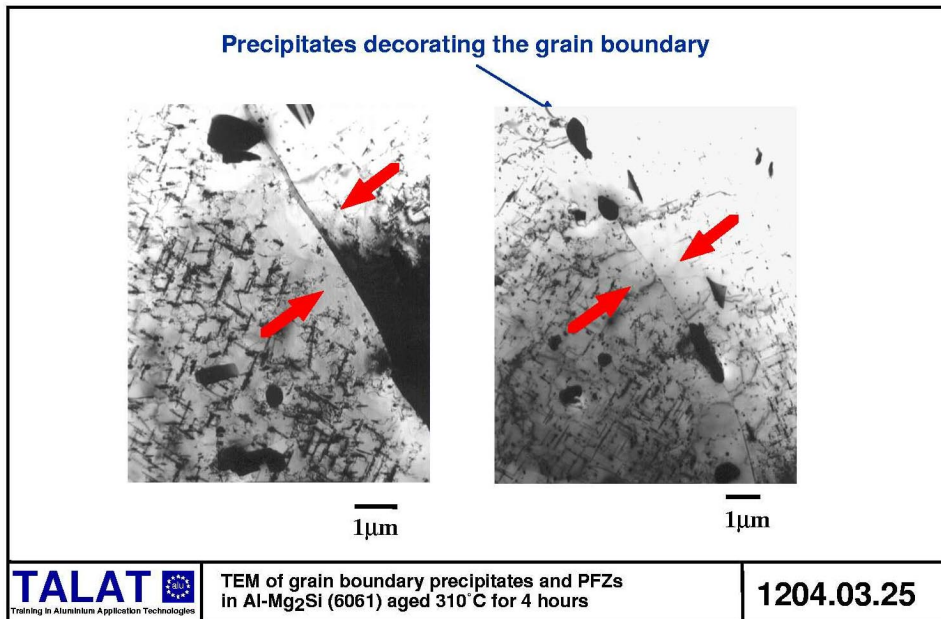
Heterogeneous nucleation is the name given to the nucleation process when it is associated with defects, such as dislocations or grain boundaries in the aluminium alloy material. The local strain field of a dislocation and the region of atomic disorder associated with a grain boundary are features that help to reduce the activation energy barrier to nucleation.

In [lecture 1201](#) we learned that a simple edge dislocation may be pictured as an extra half plane of atoms in the crystal lattice - see [Figure 1201.03.01](#); this gives rise to a lattice strain around the dislocation that varies around the dislocation from tensile to compressive. Hence, it is energetically favourable for a solute cluster with, for example a surrounding compressive strain field, to nucleate locally in the tensile strain field component of an edge dislocation. The needle-shaped clusters in Al - Mg_2Si are such an example. [Figure 1204.03.23](#) shows needles nucleated heterogeneously on a dislocation in a sample of Al - 1.2wt% Mg_2Si that was solution treated at 560°C for 1 hour, quenched into oil at 250°C and held for 10 minutes and then air cooled to room temperature; a raft of needles has grown from the dislocation. [Figure 1204.03.24](#) shows a similar sample that was stored at room temperature for 6 months and then further aged at 160°C for 24 hours; note the homogeneous precipitation and the precipitate-free zone around the raft of heterogeneous precipitates caused by local solute depletion.



The local atomic disorder associated with a grain boundary makes it energetically easier for intermediate and equilibrium precipitates to be nucleated at a grain boundary. Indeed, this is a common feature of all aluminium age hardening systems, see for example [Figure 1204.03.22](#) where zinc has precipitated on a grain boundary in an Al-Zn alloy.

See also [Figure 1204.03.25](#) which shows particles decorating a grain boundary in Al - 1.2% Mg₂Si; in this case they give rise to a narrow precipitate-free zone.

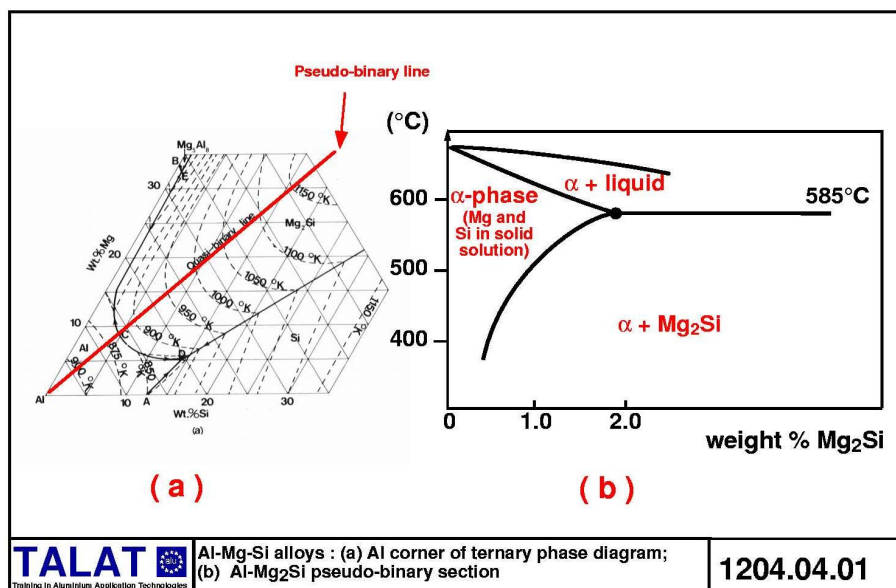


1204.04. Age Hardening - details on Al-Mg-Si

1204.04.01 Pseudo-binary Al-Mg₂Si

Al-Mg-Si alloy is a ternary system. Most engineering Al-Mg-Si alloys are based on the pseudo-binary composition Al-X% Mg₂Si. The background to ternary phase diagrams and pseudo-binary sections is given in [lecture 1203](#) and in [Figure 1203.02.01](#) and [Figure 1203.02.02](#). For convenience, the latter two figures are reproduced in

Figure 1204.04.01. The equilibrium precipitate in the Al-Mg-Si is Mg₂Si, and the so-called balanced compositions contain magnesium and silicon in same atomic ratio of 2:1 as the equilibrium precipitate. In terms of wt% this translates to the ration of 1.73:1. Compositions are then cited in terms of wt% Mg₂Si - for example, many of the results presented here refer to an Al-1.2% Mg₂Si alloy.

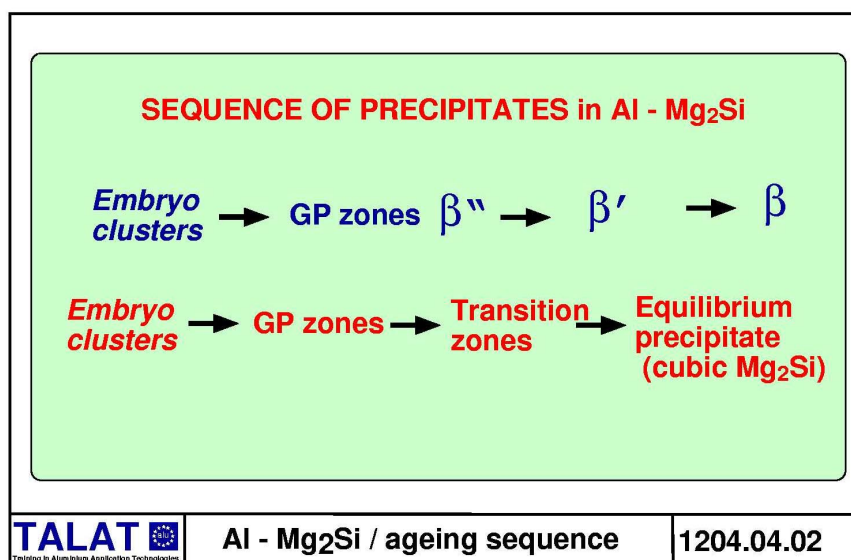


For a balanced alloy, the precipitation sequence is as shown in [Figure 1204.04.02](#), namely :

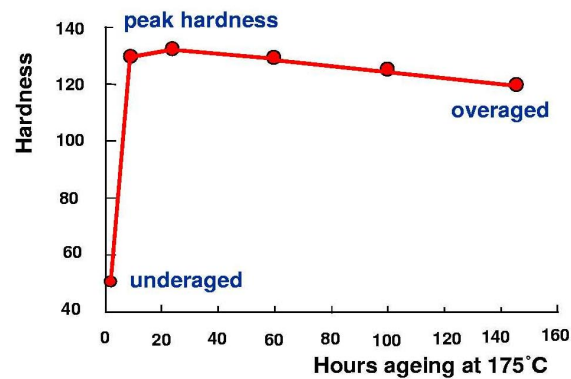
Embryo clusters → needle-shaped GP zones β'' → intermediate β' → β (Mg_2Si)

We note that the term ‘embryo cluster’ is introduced into this sequence. This is to acknowledge the recent work by Murayama et al [13] who, by using an atom probe, claim to have detected separate clusters of Mg and Si atoms. These clusters then evolve into co-clusters of Mg and Si atoms. They were not able to detect either separate clusters or co-clusters in a high resolution transmission electron microscope. The smallest clusters that can be resolved in the TEM are needle-shaped zones, which grow in length and rather more slowly in diameter, with increase in ageing time. However, the inability of TEM to detect needles at the very early stages of ageing, when there is some increase in hardness, albeit only a very small increase, is not sufficient to conclude that clustering on a scale of a few atoms is not occurring; indeed it may be concluded that clustering is occurring but on a scale which is below the resolution of the TEM.

The ageing behaviour is illustrated [14] for an Al-Mg-Si alloy 6061 which was solution treated at 530°C, water quenched and then immediately aged at 175°C. The corresponding age hardening curve is shown in [Figure 1204.04.03](#). Alloy 6061 is a balanced Al-Mg-Si alloy, with small additions of copper to improve mechanical properties and chromium to enhance corrosion behaviour. With no delay at room temperature (i.e. immediate ageing at 175°C after water quenching) the peak hardness is reached after approximately 24 hours. The corresponding TEM microstructures illustrate the GP zone (needle-shaped precipitates) that are characteristic of under ageing, peak ageing and overageing: (a) [Figure 1204.04.04](#) shows the under aged structure after 8 hours of ageing - very small needles, ~ 0.01µm in length, along <100> matrix directions are present; (b) slightly larger needles for 24 hours (peak hardness), [Figure 1204.04.05](#), and (c) further coarsened needles of for 145 hours (overaged), [Figure 1204.04.06](#).



**Solution treated at 530°C and water quenched :
no delay at room temperature, aged at 175°C**

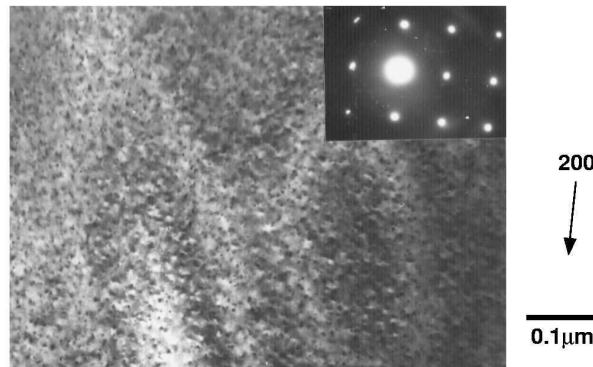


TALAT
Training in Aluminium Application Technologies

Al-Mg-Si 6061 alloy : ageing hardening
(data extracted from Z W Huang et al [14]).

1204.04.03

**Solution treated at 530°C and water quenched :
no delay at RT, aged 8 hours at 175°C (underaged)**

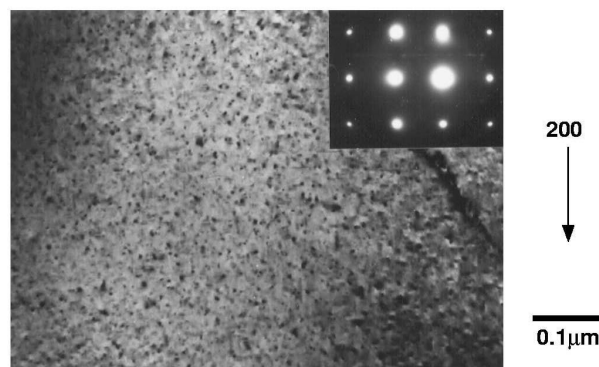


TALAT
Training in Aluminium Application Technologies

Al-Mg-Si 6061 alloy : courtesy of Dr Z W Huang

1204.04.04

**Solution treated at 530°C and water quenched :
no delay at RT, aged 24 hours at 175°C (peak hardness)**

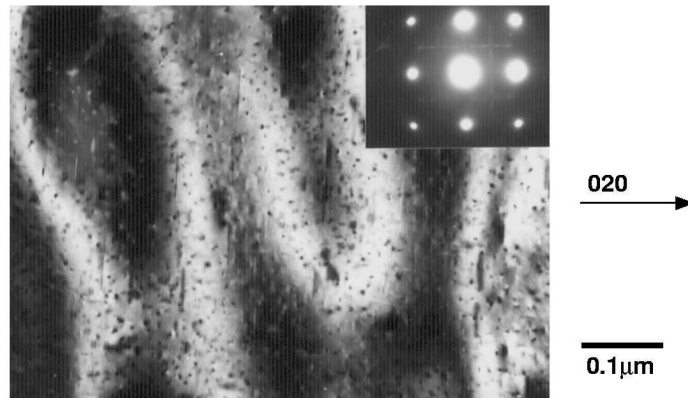


TALAT
Training in Aluminium Application Technologies

Al-Mg-Si 6061 alloy : courtesy of Dr Z W Huang

1204.04.05

**Solution treated at 530°C and water quenched :
no delay at RT, aged 145 hours at 175°C (overaged)**

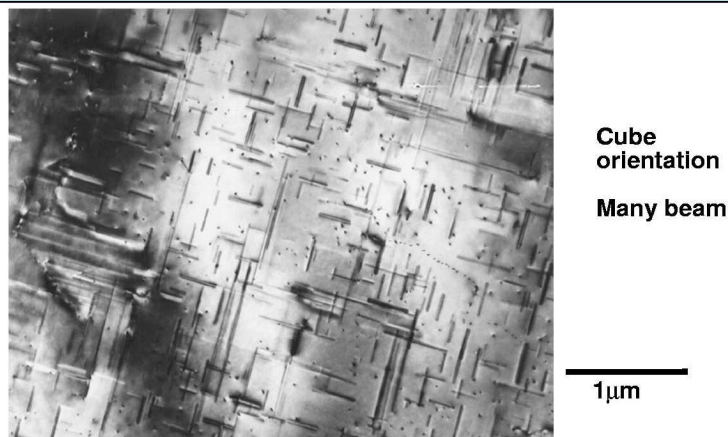


TALAT 
Training in Aluminium Application Technologies

Al-Mg-Si 6061 alloy : courtesy of Dr Z W Huang

1204.04.06

**Solution treated at 560°C and water quenched :
no delay at RT, aged 10 minutes at 200°C**

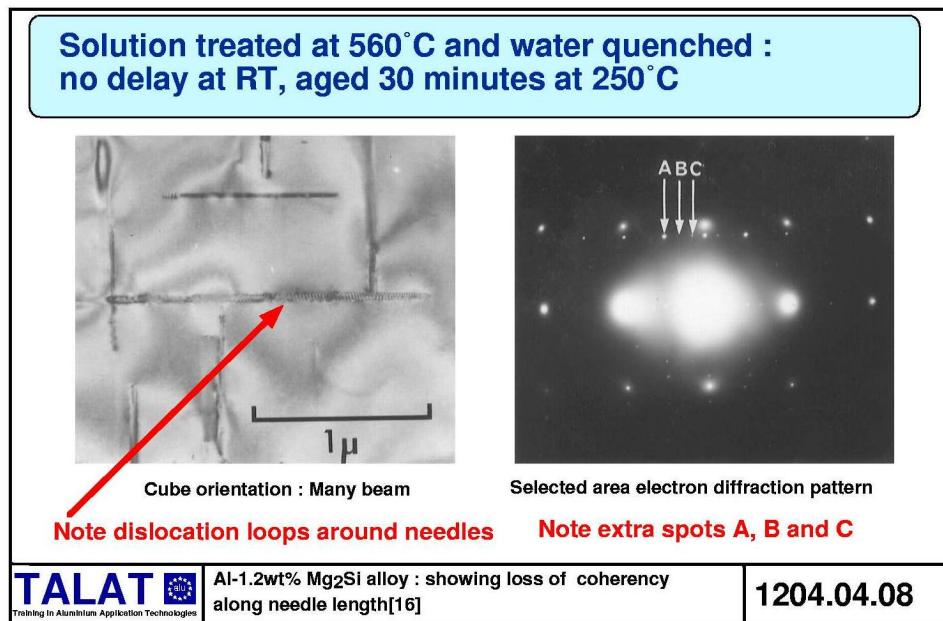


TALAT 
Training in Aluminium Application Technologies

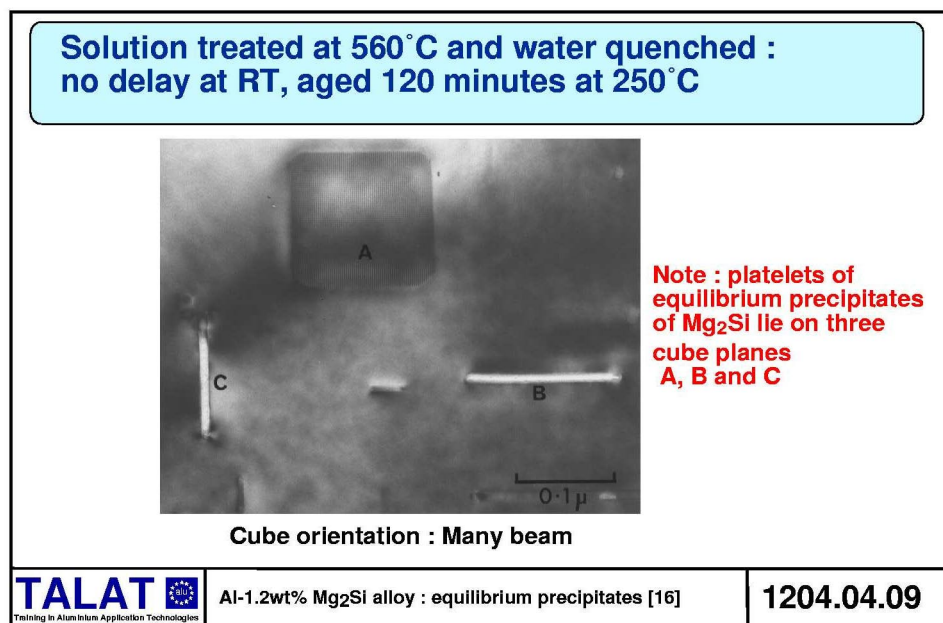
Al-1.2wt% Mg₂Si alloy : reference[16]

1204.04.07

Ageing at a higher temperature quickly leads to overaging and rapid growth of precipitate (needle) length. This is illustrated for an Al-1.2wt% Mg₂Si alloy in [Figure 1204.04.07](#) for a sample aged for 10 minutes at 200°C. Ageing for a longer time at a higher temperature, for example 30 minutes at 250°C [Figure 1204.04.08](#), leads to further growth of the needles and the formation of dislocation loops around them. This indicates that the needles have lost coherency along their length - a new intermediate phase is formed, as indicate with additional spots on the diffraction pattern.



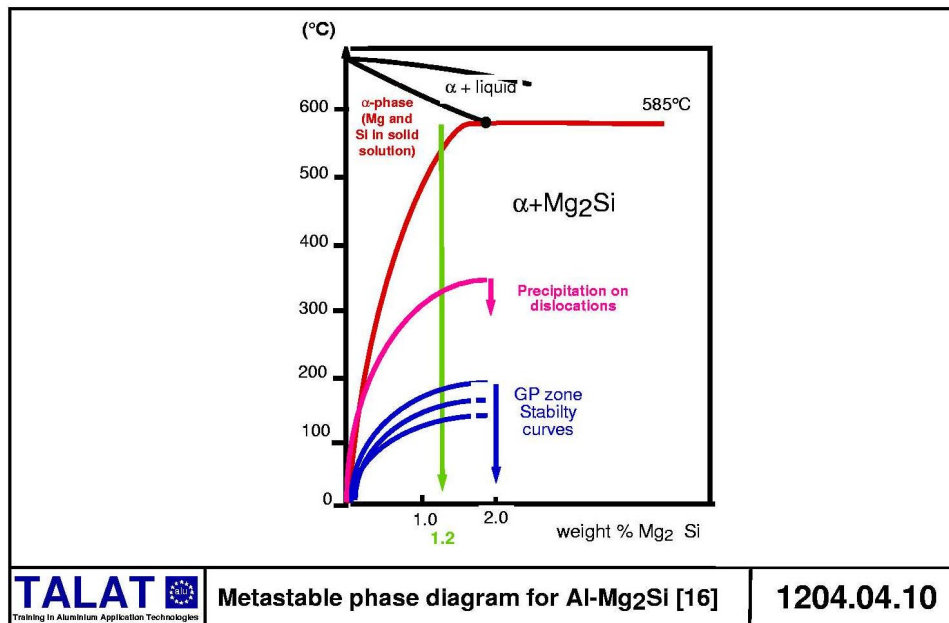
Ageing at a high temperature, say 250°C, for a long time, say 120 minutes, leads to the nucleation and growth of equilibrium precipitates of Mg₂Si. This is illustrated in [Figure 1204.04.09](#).



A GP zone solvus line cannot be readily defined for the alloy; this is because the nucleation is so dependent upon the quench rate [16]. Instead, it is more helpful to define a family of GP zone stability curves, which relate to the concentration of quenched in vacancies. So sensitive is the nucleation and stability of the GP zones to the quench rate that it seems likely that vacancies assume an important structural component of the zones; this is consistent with the recent evidence of embryo clusters at the very early stage of ageing.

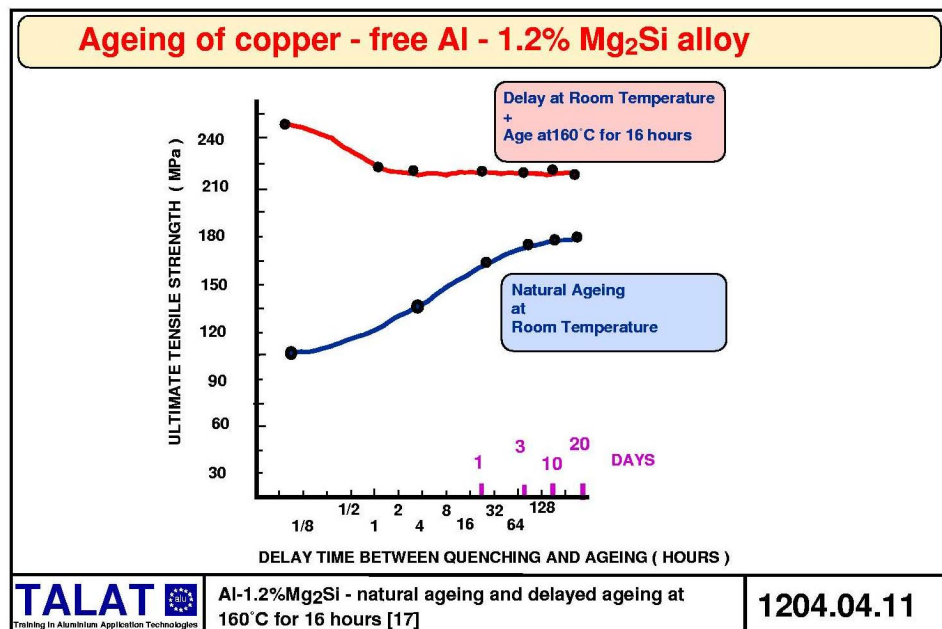
In order to aid understanding of the response of Al-Mg-Si alloys to heat treatment it is helpful to refer to the stability curves [16] shown in [Figure 1204.04.10](#); this figure

emphasises that dislocations aid the nucleation of GP zones and that much larger supersaturations are required to promote homogeneous nucleation.



1204.04.02 Natural ageing

Al-1.2% Mg₂ Si ages noticeably at room temperature [17]; see [Figure 1204.04.11](#) which shows an increase in tensile strength of > 10% after ageing at room temperature for only a few hours.



Alloys based on balanced compositions of around Al-1.2% Mg₂ Si are of industrial importance as engineering alloys processed by extrusion. Natural ageing at room temperature, caused by a period of delay between quenching after extrusion and

artificial ageing at a temperature of about 160°C, has a detrimental effect on the level of final tensile properties, [Figure 1204.04.11](#). In order to understand [16, 17, 18] the mechanisms involved, delayed ageing must be viewed as a two-step ageing process.

1204.04.03 Two step ageing

As we have seen above, the properties of Al-1.2% Mg₂Si aged at elevated temperature, eg 160°C for 16 hours, depending upon the time spent at room temperature before ageing at 160°C [17]. This type of treatment is common and should be regarded as two step ageing, [Figure 1204.04.12](#). Furthermore, Pashley et al [17] showed that an addition of 0.24wt%Cu to the alloy not only increased the level of strength at room temperature but also decreased the rate of natural ageing, [Figure 1204.04.13](#). It should also be noted that the drop-off in the values of ultimate tensile strength after two-step ageing is less marked for the copper-containing alloy for short periods of delay at room temperature.

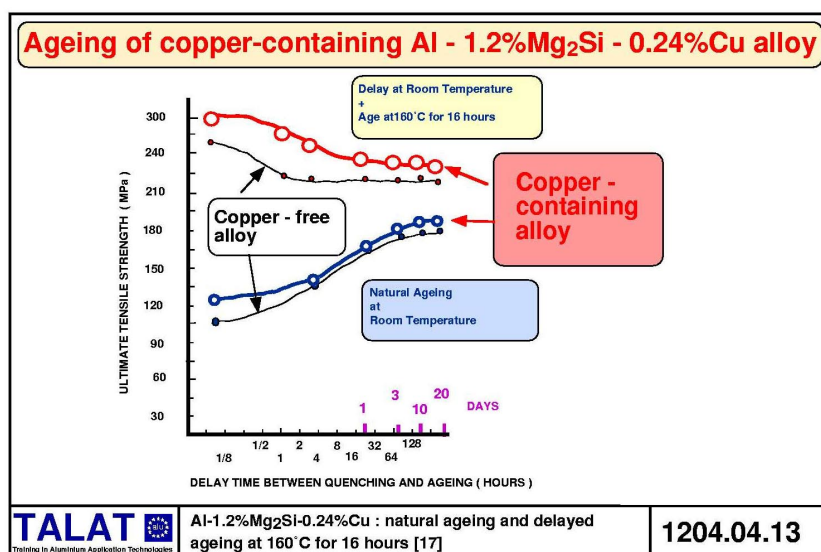
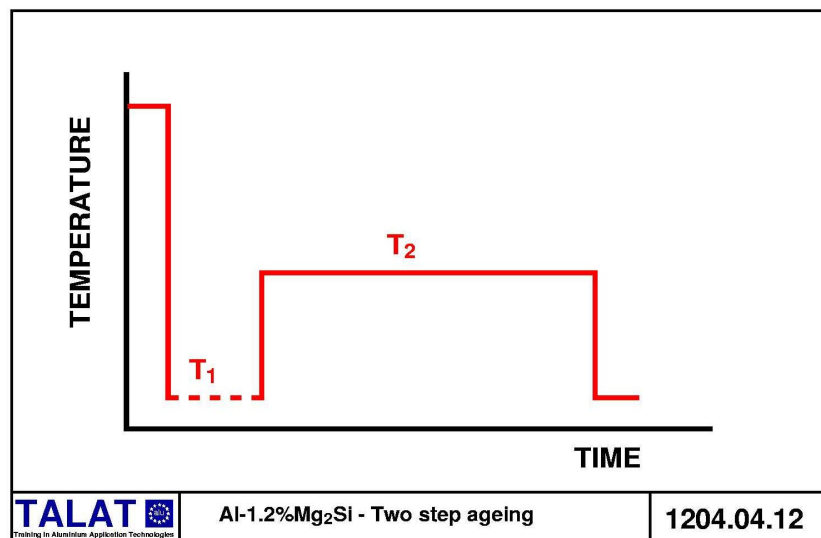
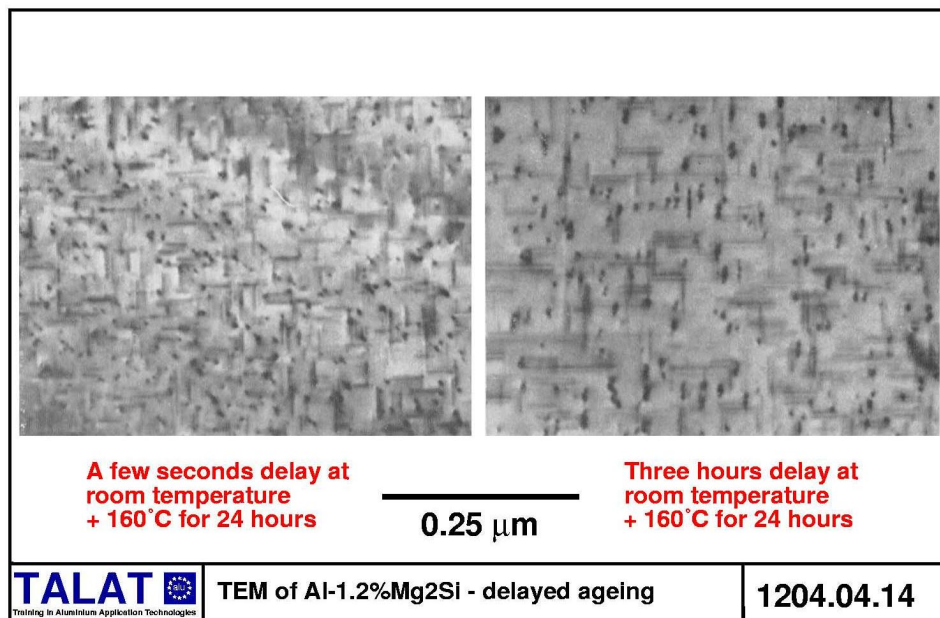


Figure 1204.04.14 shows [[17] that, for Al-1.2% Mg₂ Si, the delay at room temperature produces coarser GP zones after subsequent ageing at 160°C. The degree of coarsening measured was less in the alloy which contained 0.24%Cu, which agrees qualitatively with the observed reduced level in drop-off of tensile properties.



The mechanism of two-step ageing is described by Jacobs [16] and Pashley et al [18] and involves consideration of the influence of clustering during the delay during the first step at room temperature on the stability of clusters when the temperature is suddenly raised to the second step of artificial ageing at a higher temperature. For a very short delay of a few minutes, all of the very small clusters formed at room temperature dissolve when the ageing temperature is suddenly raised, and renucleation occurs at a density characteristic of the temperature of artificial ageing. For slightly longer delays of a few hours, a proportion of clusters formed at room temperature survive the sudden increase in ageing temperature; the cluster density is lower than that which result from a very short delay. The mechanisms involved may be seen from the following discussion, which is generalised for two-step ageing at T_1 and T_2 [16,18] :

In section 3.4.2, equation 3.4.9 was developed to give

$$r_{\text{critical}} \times \ln S_{\text{critical}} = K \quad (4.3.1)$$

where S_{critical} is the supersaturation in equilibrium with a cluster of critical radius r_{critical} at some temperature T_1 .

Hence, provided the actual supersaturation at temperature T_1 is greater than S_{critical} , then all clusters of radius greater than the critical radius r_{critical} will be stable and will grow.

However, if the temperature is increased to some higher value T_2 , then a cluster

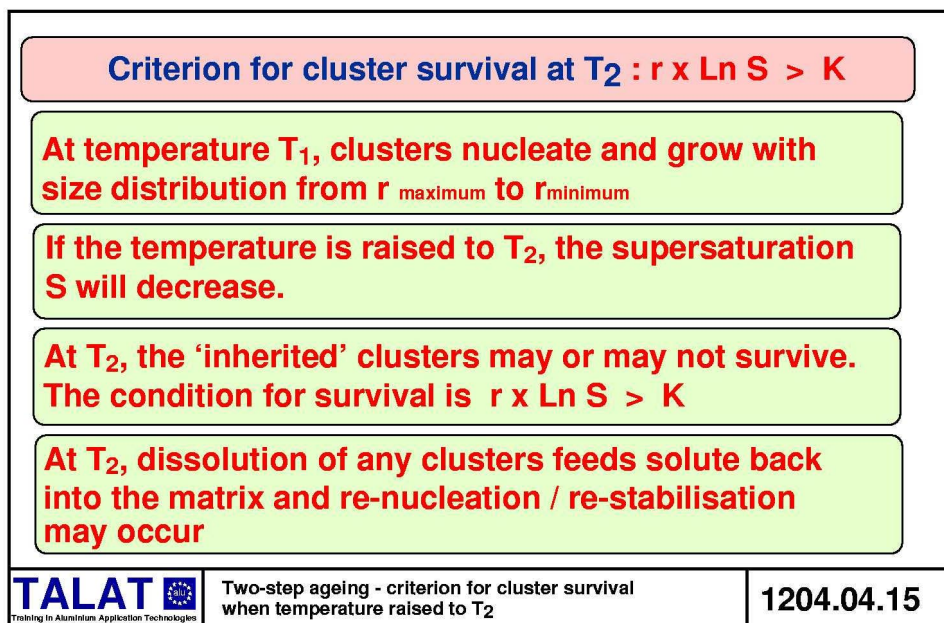
of radius r may, or may not, remain stable. We note that an increase in temperature from T_1 to T_2 must mean a decrease in effective supersaturation which, through equation 4.3.1, means that the new critical radius will be larger. Thus if r is smaller than the new critical radius then the cluster will be unstable and will dissolve. On the other hand, if r is larger than the new critical radius, the cluster will survive the increase in temperature from T_1 to T_2 and will be stable and will continue to grow. The condition for stability and continued growth is given by

$$r \times \ln S > K \quad (4.3.2)$$

where K is a temperature dependent constant.

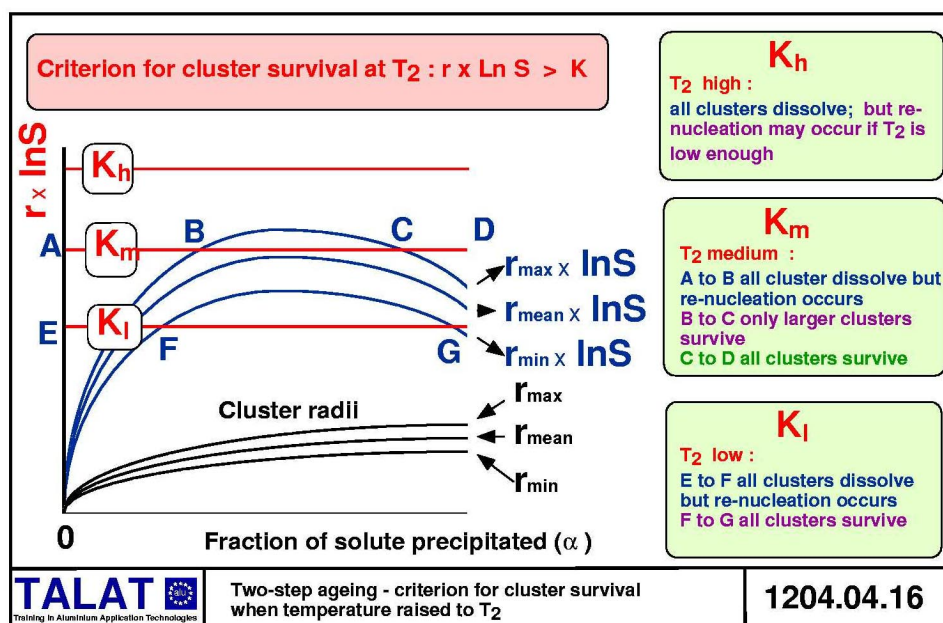
The above reasoning [16.17] may be summarised as shown in **Figure 1204.04.15**, namely

1. At temperature T_1 , clusters nucleate and grow with a size distribution from r_{maximum} to r_{minimum} .
2. If the temperature is raised to T_2 , the supersaturation S will decrease.
3. At T_2 , the 'inherited' clusters may or may not survive. The condition for survival is given by equation (4.3.2) above.
4. At T_2 , dissolution of any clusters feeds solute back into the matrix and re-nucleation / re-stabilisation may occur. NOTE : because T_2 is higher in temperature then the associated number density of clusters will be lower than those previously nucleated at T_1 .



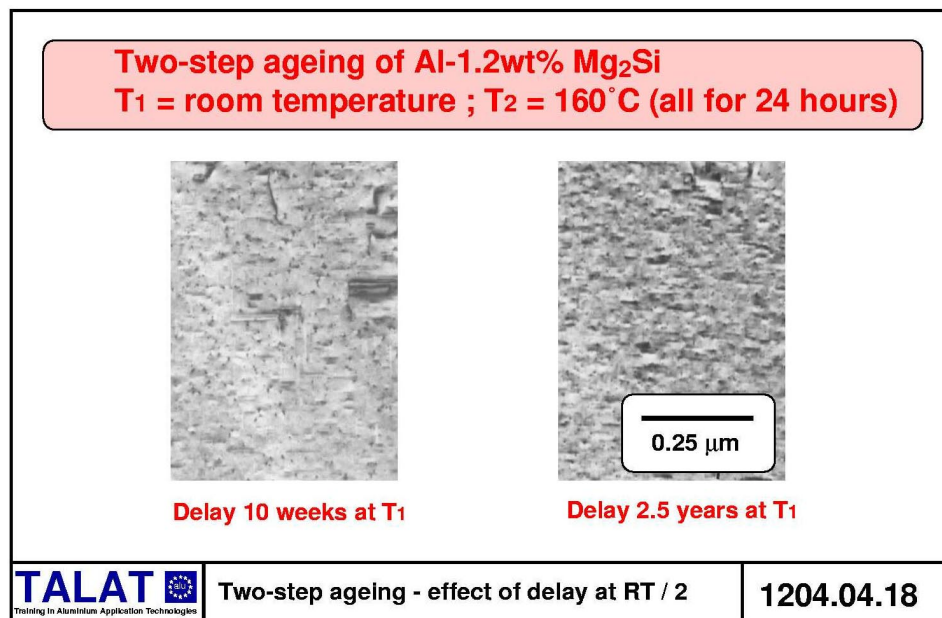
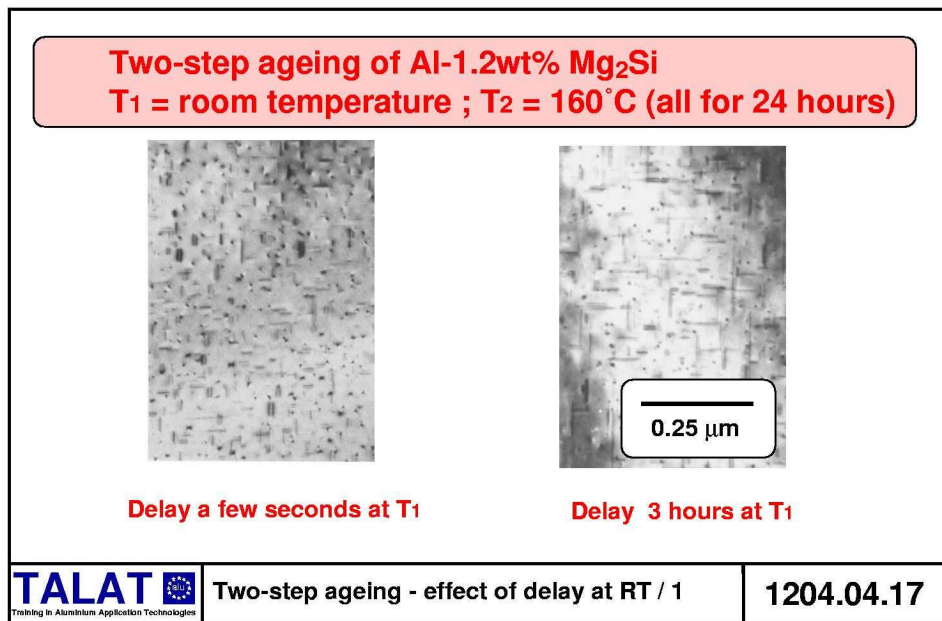
The situation is illustrated diagrammatically [16, 18] in **Figure 1204.04.16** for three different values of T_2 , high, medium and low represented by K_h , K_m and K_l . In the figure, the parameter $(r \times \ln S)$ is plotted as a function of volume fraction α of solute

remaining in solution. Thus, an increase in α is a direct result of an increase in ageing time. From this figure we note that



5. At a high value of T_2 , all clusters dissolve, but re-nucleation / re-stabilisation may occur as long as T_2 is not too high.
6. At a medium value of T_2 , between A and B all clusters dissolve but some re-nucleation / re-stabilisation may occur. Between B and C, only larger clusters survive. Between C and D all clusters survive.
7. At a low value of T_2 , between E and F all clusters dissolve but some re-nucleation / re-stabilisation may occur. Between F and G all clusters survive.

The situation described in category (6) above is illustrated in [Figure 1204.04.17](#) and [Figure 1204.04.18](#). Note the coarsening of the needles after a delay at room temperature for 3 hours. This results in the decrease in mechanical properties shown in [Figure 1204.04.13](#). Clearly, the kinetics depend upon the rate of ageing at T_1 ; in the case of the copper-containing alloy, the example shown in [Figure 1204.04.13](#), the addition of copper measurably slows the rate of natural ageing, hence the observed influence on artificial ageing - the coarsening is also delayed.



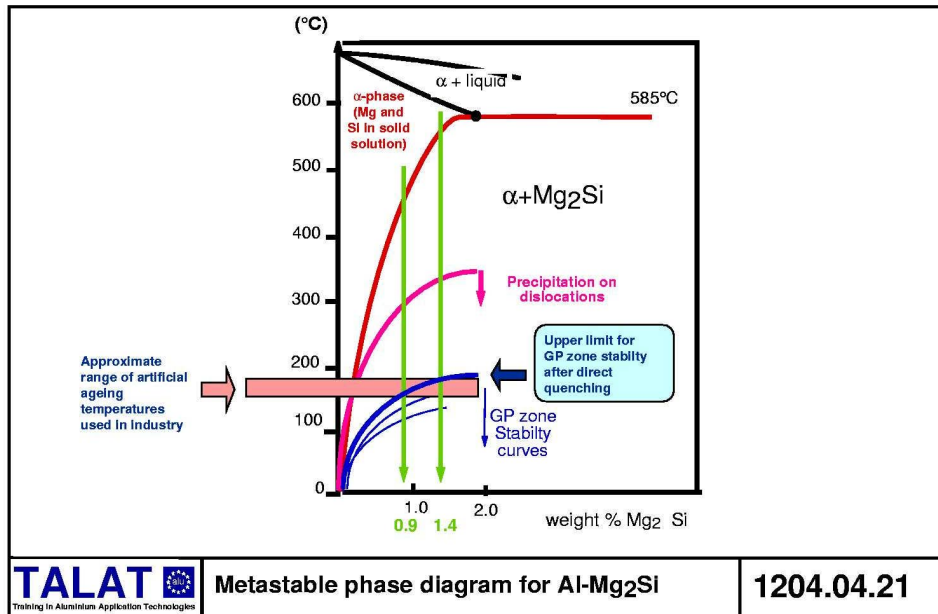
The reason why the addition of copper to an Al-1.2% Mg₂ Si alloy slows down the rate of natural ageing has not been determined. However, it may be speculated, **Figure 1204.04.19** that copper, as additional solute atoms in the alloy, becomes incorporated in the initial clustering reaction and subsequent development of GP zones. The addition of copper may also change the quantitative conditions that control GP zone stability and growth. The end result is that the rate of natural ageing is reduced, together with an overall increase in the strength levels after natural ageing and artificial ageing.

Al-1.2%Mg₂Si-0.24%Cu : mechanism of delayed ageing		
<p>The reason why the addition of copper atoms slows down natural ageing has not been determined, but it is probable that :</p> <ul style="list-style-type: none"> • Copper atoms are incorporated into to the initial clustering reaction and subsequent development of GP zones • Copper as an alloying addition modifies the thermodynamic conditions that control the nucleation and growth of zones. 		
TALAT <small>Training in Aluminium Application Technologies</small>	Al-1.2%Mg₂Si-0.24%Cu : delayed ageing	1204.04.19

There are engineering Al-Mg-Si based alloys with compositions both less than and greater than Al-1.2wt% Mg₂Si. These may be divided into three classes, **Figure 1204.04.20**, as follows:

- | | |
|---------|--|
| Class 1 | those with Mg ₂ Si less than 0.9wt% |
| Class 2 | those with Mg ₂ Si between 0.9 and 1.4 wt % |
| Class 3 | those with Mg ₂ Si greater than 1.4wt%. |

Three classes of Al - Mg₂Si		
<p>Class 1 : those with Mg₂Si less than ~ 0.9wt%</p> <p>Class 2 : those with Mg₂Si between ~ 0.9wt% and 1.4wt%</p> <p>Class 3 : those with Mg₂Si greater than ~ 1.4wt%</p>		
TALAT <small>Training in Aluminium Application Technologies</small>	Classes of Al - Mg₂Si	1204.04.20



These three classes come about as a result of the practical fact that most artificial ageing with these alloys in industry occurs in the temperature range of about 160°C to 180°C. The importance of the level of artificial ageing temperature is illustrated in [Figure 1204.04.21](#) where it will be seen that the curve for the upper limit of GP zone stability spans this temperature range for alloy compositions between about 0.9 and 1.4%. It must be emphasised that these curves are drawn [16] to represent GP zone stability after a direct quench to the ageing temperature. Of course, in practice in industry, alloys are normally quenched to room temperature and then aged - that is, they are two-step aged. Under conditions of two-step ageing, the three classes given above can be described, see [Figure 1204.04.22](#).

Three classes of Al - Mg ₂ Si		
<p>Class 1 : those with Mg₂Si less than ~ 0.9wt%</p> <p>lean alloys which depend upon seeding at RT to develop precipitation hardening during artificial ageing; kinetics depend upon quench rate</p> <p>Class 2 : those with Mg₂Si between ~ 0.9wt% and 1.4wt%</p> <p>good for extrusion since they may be water- quenched at the press ; said not to be quench- sensitive - must not be delayed excessively at RT (sensitivity reduced by copper addition)</p> <p>Class 3 : those with Mg₂Si greater than ~ 1.4wt%</p> <p>high precipitate density gives high strength, optimised by re- solution treatment and ageing ; additions of Cu and excess Si give even higher strengths; Cr sometimes added to counter adverse effect of copper on corrosion resistance</p>		
TALAT Training in Aluminium Application Technologies	Classes of Al - Mg ₂ Si	1204.04.22

Class 1 Homogeneous precipitation of GP zones in the temperature range of 160°C to 180°C will only take place if previous seeding occurs at

room temperature (there is experimental evidence to support this [18]).

- Class 2 Alloys in the approximate range 0.9 to 1.4% display the “delayed ageing” effect that is described in detail above - that is, the development of precipitation at the artificial ageing temperature is critically dependent upon the kinetics and degree of natural ageing (which are modified by an addition of copper).
- Class 3 Here, the second ageing temperature is below the upper stability curve - high precipitate densities are possible, the kinetics of nucleation and growth of which are very dependent upon the conditions of quenching.

Class 2 alloys are readily extruded. The quenching rate, although important is not super-critical as long as there is not a significant delay before artificial ageing - such alloys are said not to be very *quench sensitive*. An important processing consequence of this is that extrusions may be successfully water-quenched with a water spray upon exit from the extrusion press, thus removing the need (and expense) of a subsequent separate re-solution and quenching operation.

Class 3 alloys, with $> 1.4\%$ Mg_2Si , develop high strength upon artificial ageing, values of which are critically dependent upon the quench rate. These alloys are said to be quench sensitive. After extrusion, they are normally re-solution treated and quenched to achieve the necessary rapid quench.

The strengths of class 3 alloys may be increased by adding copper and/or excess silicon to the alloy. Chromium is sometimes added to counter the adverse effect of copper on corrosion resistance.

1204.05 Age Hardening - summary of other important engineering alloys

There are several types of wrought, heat-treatable aluminium alloys, of which the 6xxx series of Al-Mg-Si forms an industrially important part, [Figure 1204.05.01](#).

The 2xxx series, based on Al-Cu, and 7xxx series based on Al-Zn, are also important in specific areas of application. Common to 2xxx, 6xxx and 7xxx series are the temper designations reproduced in [Figure 1204.05.01](#).

[Figure 1204.05.02](#) summarises the various alloy additions that are made, in various combinations, to the base 2xxx, 6xxx and 7xxx alloys -see also TALAT [lecture 2101](#), from which the diagram is adapted.

Wrought, heat-treatable aluminium alloys	
2xxx series	Al - Cu (+ Mg)
6xxx series	Al - Mg - Si (+ Cu)
7xxx series	Al - Zn (+ Mg)

Temper designations	
	1 Partial solution treated plus natural ageing
	2 Annealed cast products only
	3 Solution treated plus cold-work
	4 Solution treated plus natural ageing
	5 Artificial aged only
	6 Solution treated plus artificial ageing
	7 Solution treated plus stabilisation
	8 Solution treated plus cold-work plus artificial ageing
	9 Solution treated plus artificial ageing plus cold-work

TALAT <small>Training in Aluminium Application Technologies</small>	Precipitation hardening alloys / 1	1204.05.01
---	------------------------------------	------------

Wrought, heat-treatable aluminium alloys	
	<p>Al - Cu</p> <ul style="list-style-type: none"> Pb and Bi (both insoluble in al) added to improve machinability Mg and Zn added to improve strength Ni and Fe added to form intermetallic which inhibits recrystallisation and grain growth Zr added to pin grain boundaries and retain very small grain size essential for superplastic deformation Li added for increased modulus and lighter weight for aerospace applications <p>Al - Mg - Si</p> <ul style="list-style-type: none"> Cu added to offset delayed ageing effect Cr added to enhance corrosion properties excess Si added to enhance tensile properties <p>Al - Zn - Mg</p> <ul style="list-style-type: none"> Cu added to obtain very high strength

TALAT <small>Training in Aluminium Application Technologies</small>	Precipitation hardening alloys / 2	1204.05.02
---	------------------------------------	------------

1204.06 Appendix Introduction to analytical electron microscopy

1204.06.01 Background

The basics of electron microscopy are summarised in [Figure 1204.06.01](#) , [Figure 1204.06.02](#), [Figure 1204.06.03](#) and [Figure 1204.06.04](#).

BASICS OF ELECTRON MICROSCOPY 1

1. Electron microscopes use electromagnetic lenses to focus beams of electrons.
2. Electrons accelerated through a potential of 100KeV and above travel through a good vacuum at a speed close to that of light.
3. The large charge to mass ratio (e/m) of an electron means that an electron beam can easily be scanned with scanning coils.
4. The very small mass of an electron means that even at a high velocity its momentum is small : bulk specimens backscatter; very thin specimens transmit electrons.

BASICS OF ELECTRON MICROSCOPY 2

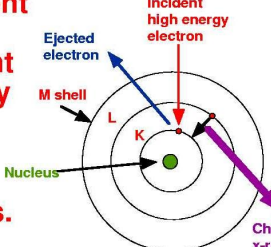
5. Electrons have wave characteristics as well as particle characteristics.
6. A 100keV electron has a wavelength λ of 0.0037nm [†] (this must be compared with the wavelength of white light at ~ 560 nm).
[†] see reference 6, page 86.
7. Why is the smallness of the electron wavelength important ?

Answer : it controls how small image details in the microscope can be resolved ie **the image resolution.**

BASICS OF ELECTRON MICROSCOPY 3

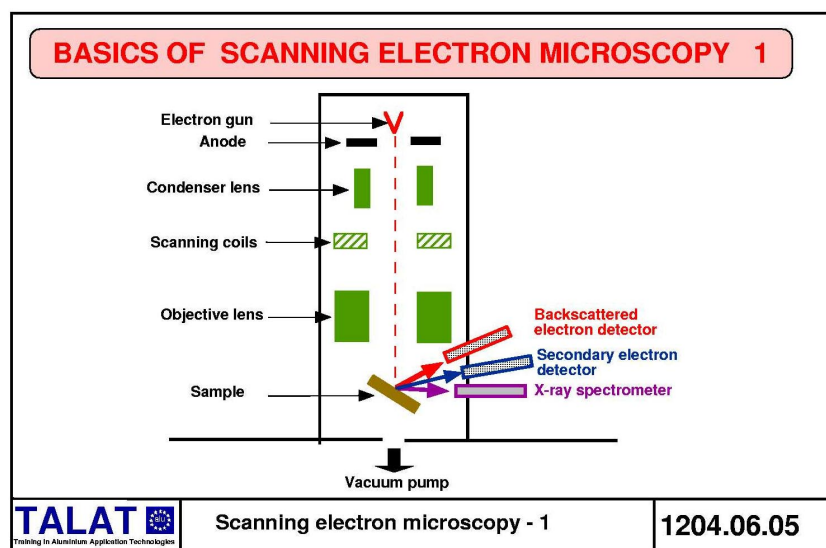
8. Going to higher and higher magnifications is of no value unless the fineness of detail in the image can be resolved.
9. For white light optical microscopy the limit of image resolution is ~ 200nm.

For 100keV electrons the limit of image resolution is ~ 1nm , or better still with modern (expensive) electron microscopes.

BASICS OF ELECTRON MICROSCOPY 4		
<p>10. When high energy electrons strike a material, the incident, high energy electrons interact with the electrons orbiting the atoms of the material.</p> <p>A number of different interactions can occur - an important one causes an x-ray to be formed.</p> <p>This is the basis of x-ray microanalysis.</p>		
		$E_x = \text{constant}$ λ_x
TALAT <small>Training in Aluminium Application Technologies</small>	Background to electron microscopy - 4	1204.06.04

1204.06.02 Scanning Electron Microscopy (SEM)

A simple diagram of a scanning electron microscope is given in [Figure 1204.06.05](#).



Polished bulk samples and fracture surfaces may be examined in the SEM.

X-ray microanalysis is limited to a resolution of $\sim 1\mu\text{m}$, [Figure 1204.06.06](#).

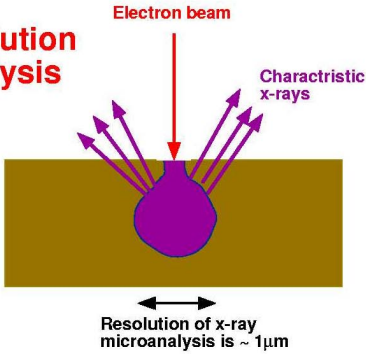
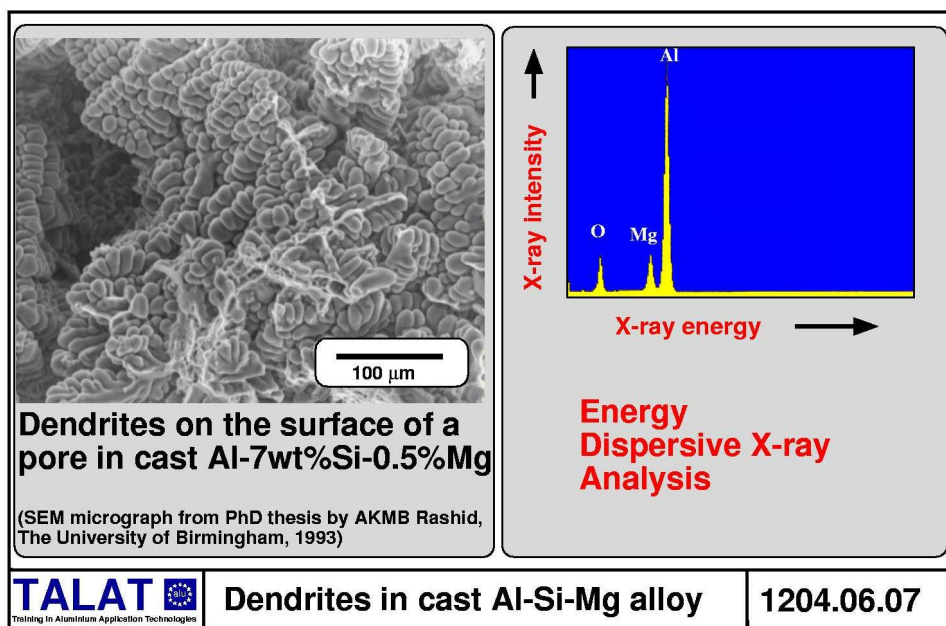
BASICS OF SCANNING ELECTRON MICROSCOPY 2		
<p>Scanned and finely focussed electron beam gives</p> <ul style="list-style-type: none"> • large depth of focus • good electron image resolution • facility for x-ray microanalysis 		
		
TALAT <small>Training in Aluminium Application Technologies</small>	Scanning electron microscopy - 2	1204.06.06

Figure 1204.06.07 shows a fracture surface of a cast Al-Si-Mg alloy which reveals the structure of an internal pore. Note that the large depth of focus reveals the dendritic nature of the internal surface of the pore. Also, from another casting with a similar pore, the X-ray spectrum allows the presence of Al, Mg and O to be detected; this confirms the presence of a trapped oxide film.



1204.06.03 Transmission Electron Microscopy (TEM)

Figure 1204.06.08 is a simple diagram of a TEM. Conditions for TEM imaging and electron diffraction are shown. Specimens for TEM must be very thin - methods of specimen preparation are summarised in [TALAT lecture 1202](#).

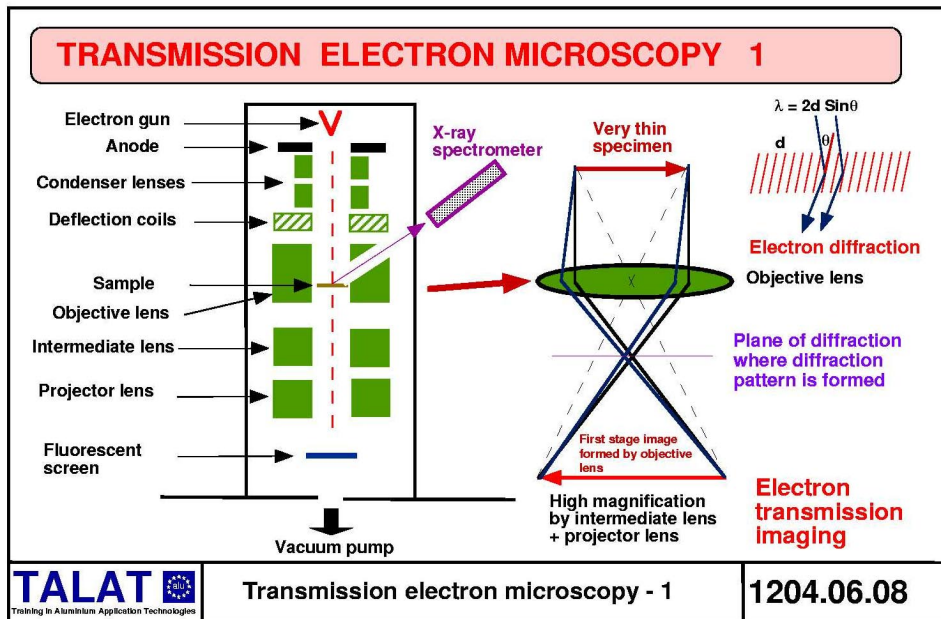


Figure 1204.06.09 is an illustration of analysis of a thin foil of Al-Cu-Li-Zr superplastic alloy. This shows very small particles of Zr-rich precipitates pinning the grain boundary. X-ray microanalysis in the TEM can be at a resolution $\sim 0.1\mu\text{m}$.

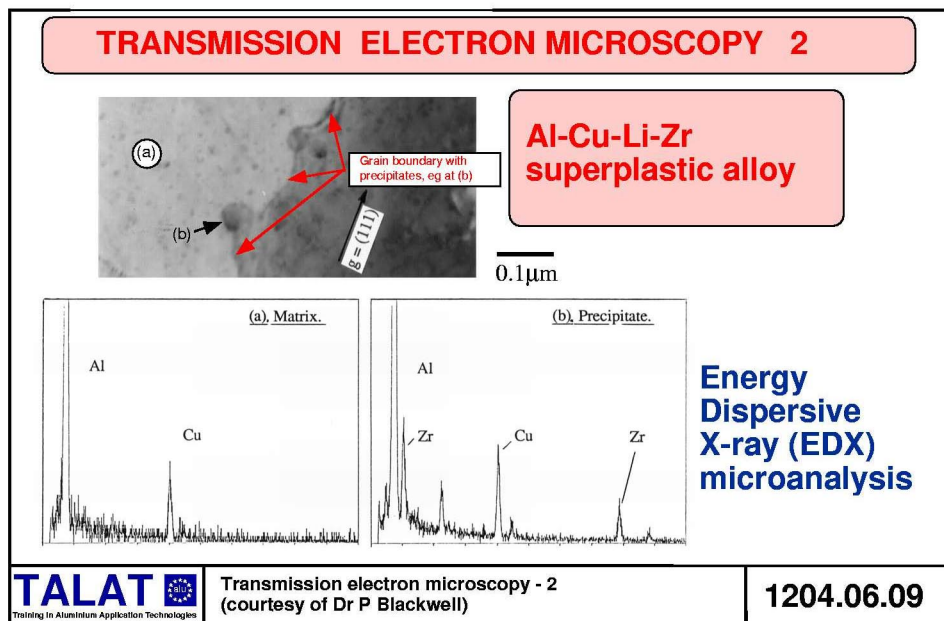
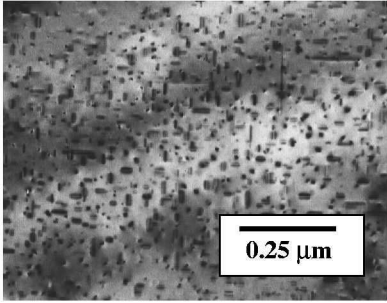
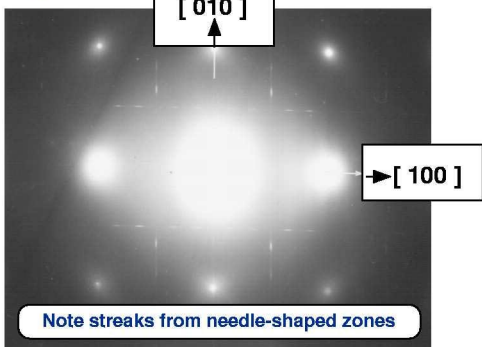



Figure 1204.06.10 shows GP zones in an Al-1.2wt% Mg_2Si alloy after a very short delay at room temperature and then aged at 160°C for 24 hours. The corresponding electron diffraction pattern is shown in the figure. The streaks on the diffraction pattern are produced by the needle-shaped GP zones - the observation that the streaks pass through the matrix reflections indicates that they are coherent with the matrix along their length [18].

TRANSMISSION ELECTRON MICROSCOPY 3		
G P Zones in Al-Mg₂Si [6xxx]		
		
Al-1.2%Mg ₂ Si aged 160°C for 24 hours : (001) electron diffraction pattern		
	Transmission electron microscopy - 3	1204.06.10

1204.07 References

1. A Wilm, *Metallurgie*, vol 8,p.225,1911.
2. P D Mercia, R G Waltenberg and R Scott, *Trans AIMME*, vol 64,p.41,1920.
3. P D Mercia, *Trans AIMME*, vol 99,p.13,1932.
4. A Guinier, *Nature*, vol 142, p,13,1938.
5. G D Preston, *Proc Roy Soc*, vol A167. p.526, 1938.
6. P B Hirsch, A Howie, R B Nicholson, D W Pashley and M J Whelan, *Electron microscopy of Thin Crystals*, Butterworth, 1965.
7. J P Lynch, L M Brown and M H Jacobs, *Acta metall.*,vol. 30, pp1389 - 1395, 1982.
8. M H Jacobs, *Phil Mag*, vol.26.,p1 , 1972.
9. D A Porter and K E Easterling, *Phase Transformations in Metals and Alloys*, Chapman & Hall, Second Edition, 1992.
10. R E Smallman, *Modern Physical Metallurgy*, Butterworth Heinemann, Fourth Edition, 1985.
11. A Kelly and R B Nicholson, *Precipitation Hardening*, Progress in Materials Science, vol.10, no.3, Pergamon, 1963.
12. M H Jacobs and D W Pashley, *The mechanism of phase transformations in crystalline solids*, Inst on Physics monograph n, 33, 1969.
13. M Murayama, K Hono, M Saga, M Kikuchi, *Materials Science and Engineering A250* (1998) pp 127-132.
14. Z W Huang, M H Loretto, R E Smallman and J White, *Mat Sci and Eng*, vol10, pp869 - 878, 1994.
15. Z W Huang, IRC, University of Birmingham, UK, *private communication*.
16. M H Jacobs, PhD thesis, *The Nucleation and Growth of Precipitates in Aluminium Alloys*, University of Warwick, 1969.
17. D W Pashley, J Rhodes and A Sendorek, *J Inst Metals*, vol. 94, Pt 2, pp 41-49, 1966.
18. D W Pashley, M H Jacobs and J T Vietz, *Phil Mag*, vol16, p51 (1967).

1204.08 List of Figures

Figure No.	Figure Title (Overhead)
1204.02.01	Precipitation hardening : Historical background
1204.03.01	Al-Rich end of Al-Cu Phase diagram
1204.03.02	Precipitation from supersaturated solid solution – clustering of solute atoms
1204.03.03	TEM image of GP zones in Al-4%Cu
1204.03.04	GP zones in Al-Cu, Al-Zn and AlMg ₂ Si
1204.03.05	TEM of spherical zones in Al-Zn
1204.03.06	TEM of rod shaped zones in Al-Mg-Si
1204.03.07	Coherency in a cubic lattice; [001] section of GP zone in Al-Cu and Al-Zn
1204.03.08	Coherency in a cubic lattice; [001] section of GP zone in Al-Mg-Si
1204.03.09	Homogeneous nucleation of a solute cluster
1204.03.10	Supersaturation and undercooling
1204.03.11	Stability of very small clusters
1204.03.12	Coarsening of solute clusters : Ostwald ripening
1204.03.13	GP zones resisting dislocation movement
1204.03.14	Typical ageing curves (I)
1204.03.15	Typical ageing curves (II)
1204.03.16	Al - Cu & Al – Zn ageing sequences
1204.03.17	TEM of Al – 4%Cu/ageing sequence (a)
1204.03.18	TEM of Al – 4%Cu/ageing sequence (b)
1204.03.19	TEM of Al – 4%Cu/ageing sequence (c) + (d)
1204.03.20	TEM of Al – 17.5% Zn; Solute depleted PFZ's
1204.03.21	TEM of Al – 17.5% Zn; Vacancy depleted PFZ's
1204.03.22	TEM of Al – 17.5% Zn; Asymmetrical PFZ
1204.03.23	TEM of precipitation on a dislocation
1204.03.24	TEM of precipitation on a dislocation + PFZ
1204.03.25	TEM of grain boundary precipitates and PFZs in Al–Mg ₂ Si (6061) aged 310°C for 4 hours
1204.04.01	Al-Mg-Si alloys : (a) Al corner of ternary phase diagram; (b) Al-Mg ₂ Si pseudo-binary section
1204.04.02	Al-Mg ₂ Si/ageing sequence
1204.04.03	Al-Mg-Si 6061 alloy : ageing hardening (data extracted from Z. W. Huang et al [14])
1204.04.04	Underaged Al-Mg-Si 6061 alloy: courtesy of Dr Z.W. Huang (TEM + diffraction pattern)
1204.04.05	Al-Mg-Si 6061 alloy with peak hardness : courtesy of Dr Z.W. Huang (TEM + diffraction pattern)
1204.04.06	Overaged Al-Mg-Si 6061 alloy: courtesy of Dr Z.W. Huang (TEM + diffraction pattern)
1204.04.07	Al – 1.2 wt% Mg ₂ Si alloy : reference [16] (TEM)
1204.04.08	Al – 1.2 wt% Mg ₂ Si alloy : showing loss of coherency along needle length [16] (TEM + diffraction pattern)
1204.04.09	Al – 1.2 wt% Mg ₂ Si alloy : equilibrium precipitates [16] (TEM)
1204.04.10	Metastable phase diagram for Al-Mg ₂ Si [16]
1204.04.11	Al – 1.2 wt% Mg ₂ Si – natural ageing and delayed ageing at 160 °C for 16

Figure No.	Figure Title (Overhead)
	hours [17]
1204.04.12	Al – 1.2% Mg ₂ Si – Two step ageing
1204.04.13	Al – 1.2%Mg ₂ Si – 0.24%Cu : natural ageing and delayed ageing at 160 °C for 16 hours
1204.04.14	TEM of Al-1.2%Mg ₂ Si – delayed ageing
1204.04.15	Two-step ageing – criterion for cluster survival when temperature raised to T ₂ (I)
1204.04.16	Two-step ageing – criterion for cluster survival when temperature raised to T ₂ (II)
1204.04.17	Two-step ageing effect of delay at RT (I)
1204.04.18	Two-step ageing effect of delay at RT (II)
1204.04.19	Al – 1.2% Mg ₂ Si – 0.24 %Cu : delayed ageing
1204.04.20	Classes of Al – Mg ₂ Si alloys
1204.04.21	Metastable phase diagram for Al-Mg ₂ Si
1204.04.22	Classes description of Al-Mg ₂ Si alloy
1204.05.01	Precipitation hardening alloys (I)
1204.05.02	Precipitation hardening alloys (II)
1204.06.01	Background to electron microscopy (I)
1204.06.02	Background to electron microscopy (II)
1204.06.03	Background to electron microscopy (III)
1204.06.04	Background to electron microscopy (IV)
1204.06.05	Scanning electron microscopy (I)
1204.06.06	Scanning electron microscopy (II)
1204.06.07	Dendrites in cast Al-Si-Mg alloy
1204.06.08	Transmission electron microscopy (I)
1204.06.09	Transmission electron microscopy (II)
1204.06.10	Transmission electron microscopy (III)